Mixed coagulant-flocculant optimization for pharmaceutical effluent pretreatment using response surface methodology and Gaussian process regression

H. Tahraoui, A.-E. Belhadj, Z. Triki, N.R. Boudellal, S. Seder, A. Amrane, J. Zhang, N Moula, A. Tifoura, R. Ferhat, et al.

Mixed Coagulant-flocculant optimization for pharmaceutical effluent pretreatment using response surface methodology and gaussian process regression

Hichem Tahraoui [a*], *Abd-Elmouneïm Belhadj* [a], *Zakaria Triki* [a], *Nihel Rayen Boudella* [b], *Sarah Seder* [b], *Abdeltif Amrane* [c], *Jie Zhang* [d], *Nassim Moula* [e], *Amina Tifoura* [f], *Radhia Ferhat* [g], *Abla Bousselma* [h] *and* , *Nadia Mihoubi* [i]

[a] Laboratory of Biomaterials and Transport Phenomena (LBMPT), University of MÉDÉA, ALGERIA, Nouveau Pôle Urbain, Médéa University, 26000 Médéa, Algeria. E-mail: tahraoui.hichem@univ-medea.dz , belhadj_1@yahoo.fr , triki.zakaria@univ-medea.dz, URL: www.univ-Médéa.dz .

[b] Technological Hall, Faculty of Technology, University Yahia Fares of Médéa, 26000, Algeria. E-mail: mboudellalnihel@gmail.com , msarasdr25@gmail.com , URL: www.univ-Médéa.dz

[c] Univ Rennes, Ecole Nationale Supérieure de Chimie de Rennes, CNRS, ISCR – UMR6226, F-35000 Rennes, France. E-mail: abdeltif.amrane@univ-rennes1.fr, URL: www.univ-Rennes1.dz

[d] School of Engineering, Merz Court, Newcastle University, Newcastle upon Tyne NE1 7RU, UK. E-mail: jie.zhang@newcastle.ac.uk URL: www.ncl.ac.uk

[e] Fundamental and Applied Research in Animal and Health (FARAH) Department of Veterinary Management of Animal Resources, Faculty of Veterinary Medicine, University of Liege, Liege 4000, Belgium. E-mail: nassim.moula@uliege.be URL: www.uliege.be

[f] Biology laboratory, Faculty of Science, University Yahia Fares of Médéa, 26000, Algeria. E-mail: amitifoura@gmail.com , URL: www.univ-Médéa.dz

[g] Laboratory of Food Science (LSA), Food Engineering Department, University of Batna 1 Hadj Lakhdar, Biskra Avenue, Batna, 05005, Algeria. E-mail: radhia.ferhat@univ-batna.dz , URL: www.univ-batna.dz.

[h] Laboratory (LAPAPEZA), Food Engineering Department, University of Batna 1 Hadj Lakhdar, Biskra Avenue, Batna, 05005, Algeria. E-mail: abla.bousselma@univ-batna.dz , URL: www.univ-batna.dz.

[i] Materials and Environmental Laboratory (LME), University of MÉDÉA, ALGERIA, Nouveau Pôle Urbain, Médéa University, 26000 Médéa, Algeria. E-mail: nadiamihouona@gmail.com , URL: www.univ-Médéa.dz.

[*] Corresponding Author: Hichem Tahraoui, tahraoui.hichem@univ-medea.dz

Abstract

Wastewater from the Antibiotical-Saidal pharmaceutical plant (Medéa) was pretreated by coagulation-flocculation using copper sulfate ($CuSO_4$), iron chloride ($FeCl_3$), and mixture of the two salts combined in a 1:1 (v/v) ratio in the present study. Response surface methodology (RSM) was used to optimize pH and coagulant dosage as independent variables, while dissolved organic carbon (DOC), absorbance at 254 nm (UV 254), and turbidity were provided as dependent variables in the central composite design (CCD). Then, the databases of the three treatments were combined in a single database to create a general model valid for the three treatments at the same time, and to predict the reduction rates of DOC, UV254, and turbidity, using the Gaussian process regression coupled with the dragonfly optimization algorithm (GPR-DA).

To have the best model obtained between RMS and GPR-DA, an experimental validation was carried out after having had the optimal conditions of each type of coagulant, using the multi-objective optimization technique. The results of the experimental validation show the superiority of the GPR-DA model compared to the RSM model. Also, the results show that the mixed coagulant ($CuSO_4$+ $FeCl_3$) obtain better results than $CuSO_4$ or $FeCl_3$ alone with a treatment efficiency equal to 92.68% at pH = 5 and dosage = 600 mg/L, and the reductions in DOC, UV 254 and turbidity are 97.32%, 82.90% and 96.47%, respectively.

Graphical Abstract

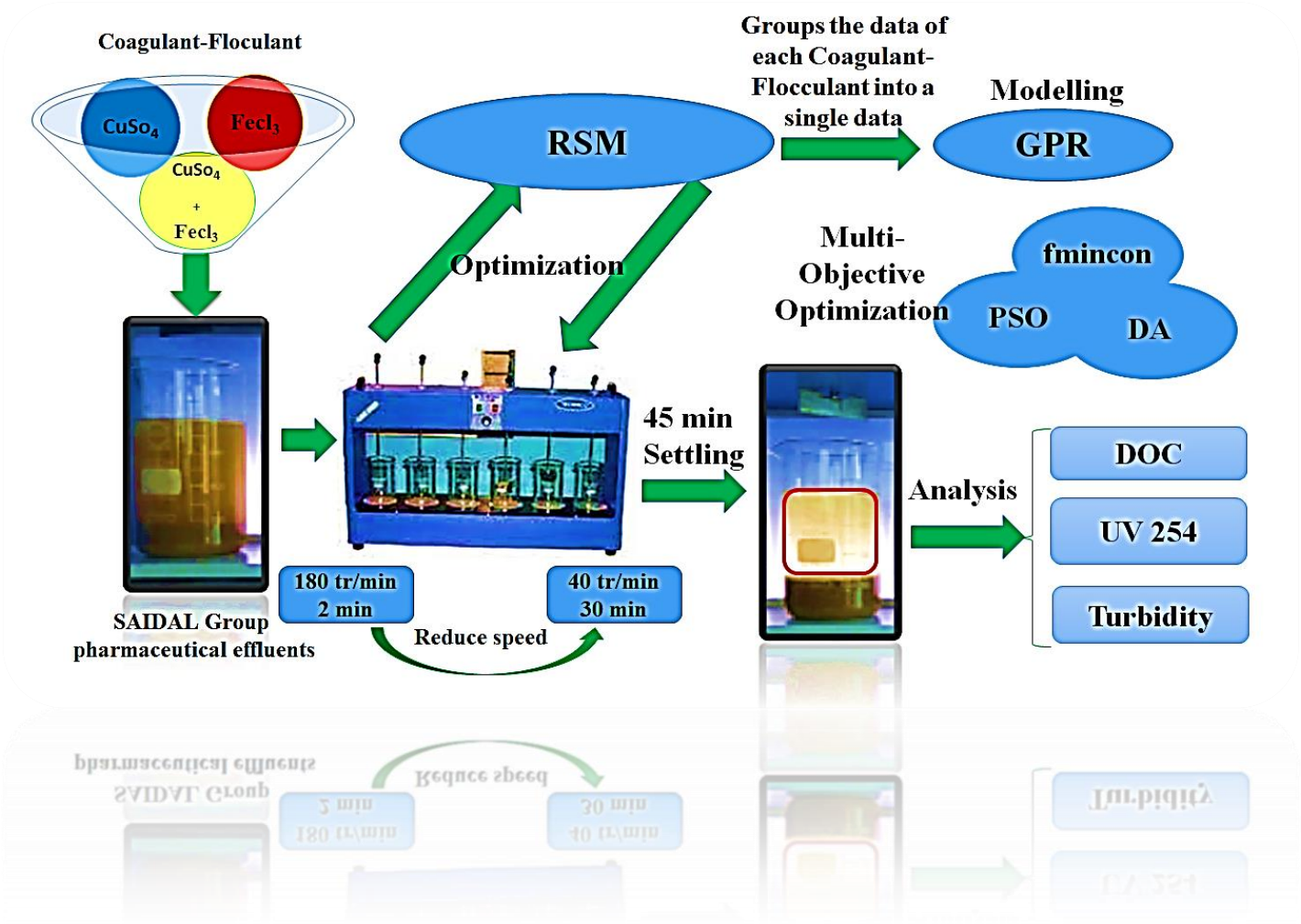

Keywords

Pharmaceutical effluent, Coagulation-flocculation, Response surface methodology, Gaussian process regression, Multi-objective optimization.

1. Introduction

In recent years, the pharmaceutical industries have experienced intense development due to population growth and enormous public health needs (Gadipelly et al., 2014; Ng et al., 2016; Qian et al., 2019), which has also led to an increase in production and consequently an increase in associated wastewater discharges affecting natural resources (Ghumra et al.,

2021; Rawat, 2019). These effluents, if not adequately treated, become a significant source of micro-contaminants in the environment, resulting in harmful impacts on aquatic life and human health, such as water toxicity, pathogenic bacteria, and genotoxicity (Kumar et al., 2010; López-Fernández et al., 2012; Qian et al., 2019). Pharmaceutical wastewater contains complex mixtures of chemicals, intermediates, solvents, acids, alkalis, and many industry-specific additives used in manufacturing different pharmaceuticals (Lalwani et al., 2020). As a result, the wastewater generated may contain colors, odors, dissolved and suspended solids, inorganic chemicals, high turbidity, dissolved organic carbon, volatile organic compounds (VOCs), heavy metals, micro and macro pollutants specific to the industry; likewise, there are significant quantities of biological compounds, solvents, and catalysts that are poisonous and resistant to biodegradation (Gadipelly et al., 2014; Lalwani et al., 2020; Qian et al., 2015; Sreekanth et al., 2009). These complex mixtures are characterized by very high organic resistance (mainly provided by various organic solvents), high salinity, low biodegradability, and a wide pH range (Changotra et al., 2019a; Jose and Philip, 2021; Kaya et al., 2017). All these make pharmaceutical wastewater treatment very difficult and, as a consequence, pharmaceutical wastewater treatment methods are extensively studied with a view to effectively reduce pollution. This is part of a promising strategy to reduce water shortages and, above all, an essential step for addressing environmental issues (Chen et al., 2020), but also for emerging uses of water in the technological field (Boldrini et al., 2017; Changotra et al., 2019b; Santhosh et al., 2016; Wu et al., 2017). Thus, wastewater treatment plants have been installed in every industry to improve ecosystem and human health and help to support water harvesting (Ho et al., 2019).

According to the literature (Shahedi et al., 2020), wastewater treatment methods could be classified into three main categories: physical, chemical, and biological processes. Among

these, biological treatments remain the most widely used wastewater treatment process at pilot and industrial scale due to their environmentally friendly operations and cost-effectiveness (Benitez et al., 2001; El-Din and Smith, 2002). Biological activities are successful in eliminating the majority of organic pollutants and ammoniacal nitrogen from the environment. Svojitka et al. (2017) reported a chemical oxygen demand (COD) removal efficiency of 78 % in a pilot anaerobic membrane bioreactor for post-pharmaceutical wastewater treatment. Rao et al. (2005) show that fixed-film reactors can remove 60 to 70 % of the organic matter from the wastewater when the organic input rate is 10 g DOC/L/day. However, the limited treatment effectiveness of existing wastewater treatment plants in degrading recalcitrant and toxic pharmaceutical wastewater has led to the exploration of more radical pharmaceutical wastewater treatment methodologies to improve the biodegradability of wastewater before biological treatment (Changotra et al., 2019b). Indeed, multiple studies have indicated that various biological systems may be unable to break down weakly biodegradable, resistant, and refractory substances (Lapworth et al., 2012; Prieto-Rodríguez et al., 2013; Tran et al., 2014). As a result, Liu et al. (2012) reported that contents of medicines were discovered in sewage treatment plant effluents and also that pharmaceutical compounds were detected in surface water, soil and groundwater even after biological treatments (Joss et al., 2006; K'oreje et al., 2016). It is also revealed that the use of biological treatment processes in the presence of antibiotics creates long-term antimicrobial resistance (Lalwani et al., 2020; Zhou et al., 2006).

Several wastewater processing processes can be combined for more efficiency to overcome this problem. However, the complete treatment of wastewater generally requires many steps (Sher et al., 2013). Due to the chemical stability and the low biodegradability of several organic pollutants, e.g. Hormones, biological treatments have generally been coupled as a complementary treatment step to attempt to overcome the reduced efficacy of

conventional treatment methods (Cheng et al., 2020; Rodrigueza et al., 2016; Yarahmadi et al., 2018). Various combinations of conventional wastewater treatment processes have been used, such as coagulation (Changotra et al., 2019b), adsorption (Carvalho et al., 2012), membrane filtration (Ganiyu et al., 2015), incineration (Mu et al., 2012), and as well as biological treatments coupled with coagulation and flocculation processes for the treatment of pharmaceutical wastewater (Changotra et al., 2019b; Pal, 2018).During coagulation-flocculation treatments, the addition of chemicals modifies the physical state of the dissolved and suspended solids and promotes the removal of these solids by precipitation (Ashraf et al., 2016). The suppression mechanism of this process is mainly due to the load neutralization of the colloids charged negatively by cationic hydrolysis products, which allows the initial aggregation of colloidal particles to form micro-flakes (Sher et al., 2013). In addition, coagulation is a treatment that can reduce the turbidity and the elimination of the color and pathogens (Ashraf et al., 2016), as well as the elimination of organic matter (Ashraf et al., 2016). The effectiveness of the coagulation-flocculation process depends on several factors, including the type of coagulant, dosage, pH, temperature, ionic strength, nature and concentration of organic matter, the total dissolved solids, as well as the size and distribution of colloidal particles in suspensions (Sher et al., 2013). The most used coagulants are iron and alum salts. These coagulants favor the agglomeration of the particles by reducing the electrostatic charges of the surface of the particles in the acid pH region where the hydrolyzed metal species are plentiful (Santo et al., 2012).

Coagulation/flocculation have been reported as an effective method in the treatment of wastewater in many industries such as: the treatment of minerals, metallurgy, and textile, the treatment of Tannery effluents, yeast wastewater, textile, petroleum refinery, dyeing

bath and dyeing house, aquaculture, vinassas, municipal, lixivitations, poll page, mill with olives and many others (Sher et al., 2013).

For this purpose, many researches on the development of coagulation-flocculation methods for the treatment of industrial effluents primarily aimed at performance optimization have been in progress (Adesina et al., 2019; Tahraoui et al., 2021b; Trinh and Kang, 2011).

Various methods of optimizing the wastewater treatment methods have been used in recent decades to improve the process performance, such as Response Surface Methodology (RSM) shown in Table 1.

In this research, the potential and efficiency of a coagulation and flocculation process using copper sulfate ($CuSO_4$), ferric chloride ($FeCl_3$), and a combination of cupric sulfate and ferric chloride in a ratio of 1:1 ($CuSO_4$+ $FeCl_3$) for the pretreatment of pharmaceutical industrial effluents are investigated. The models created using RSM with central composite design technique (CCD) are used to optimize the treatment condition. Before and after the tests, the dissolved organic carbon (DOC) in the water, the absorbance at 254 Nm (UV 254), and the turbidity were measured. The two variables (pH and coagulation dosages) and the three responses (DOC, turbidity, and UV 254) were taken into account to find the best treatment condition. Then, the Gaussian process regression model coupled with the dragonfly optimization algorithm (GPR-DA) was used to model the three outputs after combining the databases from the three treatment approaches. Afterwards, multi-objective optimization procedures by using three techniques (fmincon, dragonfly and particle swarm) were carried out to find the optimal treatment conditions. Finally, an application was created using the MATLAB guide to provide a simple way to implement Multi-Objective Optimization (MOO) and predict DOC, UV254, turbidity and treatment efficiency. To our knowledge, optimizing the efficiency of coagulants flocculant used to pre-treat pharmaceutical effluents derived from RSM and GPR-DA has never been

attempted before. Moreover, comparison of the MOO approaches has never been made before in this context.

The article is organized as follows. Section 2 presents the treatment of liquid effluent from the pharmaceutical plant by two individual coagulants/flocculants and their mixture and the experiments carried out using RSM and CCD. Then models are developed from the experimental data by using Gaussian process regression coupled with the dragonfly (GPR-DA). Based on the developed models, MOO based on three algorithms was performed to find the optimal treatment condition. Section 3 presents a comparison between the two individual coagulants/flocculants and their mixture in order to find the best treatment approach. The MOO results are validated through experiments. The last section concludes the paper.

Table 1 – Reviewed Research Articles on Optimizing Wastewater Treatment by RSM.

Article titles	Contributions and limitations	References
Response surface methodology approach to optimization of process parameter for coagulation process of surface water using Moringa oleifera seed	This study focused on the use of Moringa oleifera seeds as a coagulant for surface water treatment using RSM. Four factors were evaluated, namely the stabilization time, the stirring time, the stirring speed and the concentration of Moringa oleifera seed extract. The model predicts the lowest turbidity of 5.49 NTU with optimal conditions of stabilization time of 120 min, stirring speed of 100 rpm, stirring time of 10 min and coagulant concentration of 3 g/L. Despite the good results obtained in this study in terms of	Adesina et al., 2019

	turbidity elimination, this method remains limited by the high costs of operation and preparation of Moringa oleifera seeds. Furthermore, the dose of Moringa oleifera used in this treatment is very high (3g/L) compared to other coagulants such as aluminum sulfate which generally does not exceed 1g/L and with an effective very high turbidity removal (Tahraoui et al., 2021b; Trinh and Kang, 2011). In addition, this study only focused on the removal of turbidity from the raw water of the Nakdong River and the method cannot be used in the treatment of pharmaceutical effluents.	
Response surface methodological approach to optimize the coagulation–flocculation process in drinking water treatment	RSM was used in this work to find the optimal combination of coagulant dose and pH with respect to the highest turbidity and organic carbon removal efficiency dissolved (DOC). The results obtained with polyaluminium chloride (PACl) were compared with those obtained using a conventional coagulant such as aluminum. Quadratic models developed for the two responses (turbidity removal and DOC removal) indicated that the optimal conditions for a PAC1 concentration of 0.11 mM at pH	Trinh and Kang, 2011

	7.4 and an alum concentration of 0.15 mM at pH 6.6. The compromise to optimize both responses simultaneously resulted in 91.4% turbidity removal and 31.2% DOC removal using PACl, while removals using aluminum were 86.3% turbidity and 34.3% DOC. This study remains very weak to apply to the treatment of water loaded with organic matter, in particular for the treatment of pharmaceutical effluents. Because the two coagulants used in this study gave a very low DOC removal rate, the removal rate did not exceed 34.3% at treated water DOC values of 3.69 – 3.76 mg/L.	
Optimisation and Prediction of the Coagulant Dose for the Elimination of Organic Micropollutants Based on Turbidity	RSM was applied to optimize and prediction the coagulant dose for the removal of organic micropollutants based on turbidity. The water contaminated with humic acid was treated using the aluminum sulfate coagulant according to pH, temperature, conductivity, turbidity and Total alkalimetric titre. The results show a very high treatment efficiency of 99.96% using coagulation with a dosage of 109.50 mg/L.	(Tahraoui et al., 2021b)
	The results of this method are very interesting	

to apply in the field of treatment of pharmaceutical effluents. But, this method is limited by many of the inputs used., as the interaction effect of the independent variables and the collaborative analysis between a large number of independent and dependent variables becomes difficult for accurate optimization (Singh and Kumar, 2020a). This poses a difficult control problem because it is nonlinear and complex (Tahraoui et al., 2021b).

2. MATERIALS AND METHODS

2.1. Collection of wastewater samples

In Algeria, the Saidal Group Medicine Production Factory is a stock company with a capital of 2.5 billion Algerian dinars. The State holds 80% of the capital of the Saidal Group, and the remaining 20% were assigned in 1999 to institutional investors and natural persons (www.saidalgroup.dz). It contains several subsidiaries on the national territory: Biotic subsidiary, Farmall subsidiary, antibiotic subsidiary, and others. Figure 1 shows the different subsidiaries, their location, and drugs manufactured in the company (GROUPE, 2001).

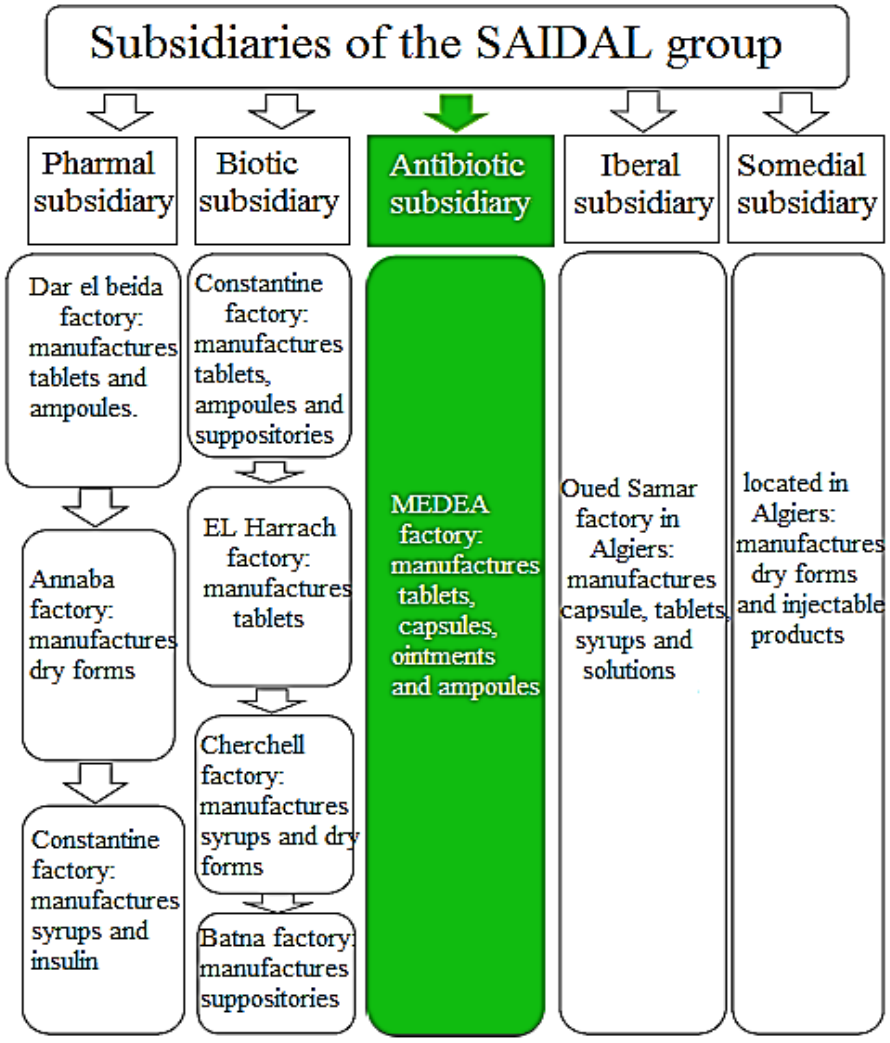

Figure 1 – Characterization of the different subsidiaries of the SAIDAL group in Algeria.

In this study, the wastewater was collected for one month from the rejection of the medéa antibiotic complex (Figure 2) before returning to to the treatment plant, and the selection of this site is because the wastewater from this site is difficult for biological degradation. The effluents from this type of plants are less biodegradable (Lapworth et al., 2012; Prieto-Rodríguez et al., 2013; Tran et al., 2014), and also the presence of antibiotics creates long-term antimicrobial resistance (Lalwani et al., 2020; Zhou et al., 2006). It should be noted that this subsidiary is located in Médéa, about 80 km west of Algeria (Iguergaziz et al., 2019), and it started in 1986 specializing in the production of penicillinic and non-penicillinic antibiotics for anti-inflammatory and antipyretic (www.saidalgroup.dz). It has

facilities needed to manufacture drugs from obtaining the active ingredient until its galenic formatting.

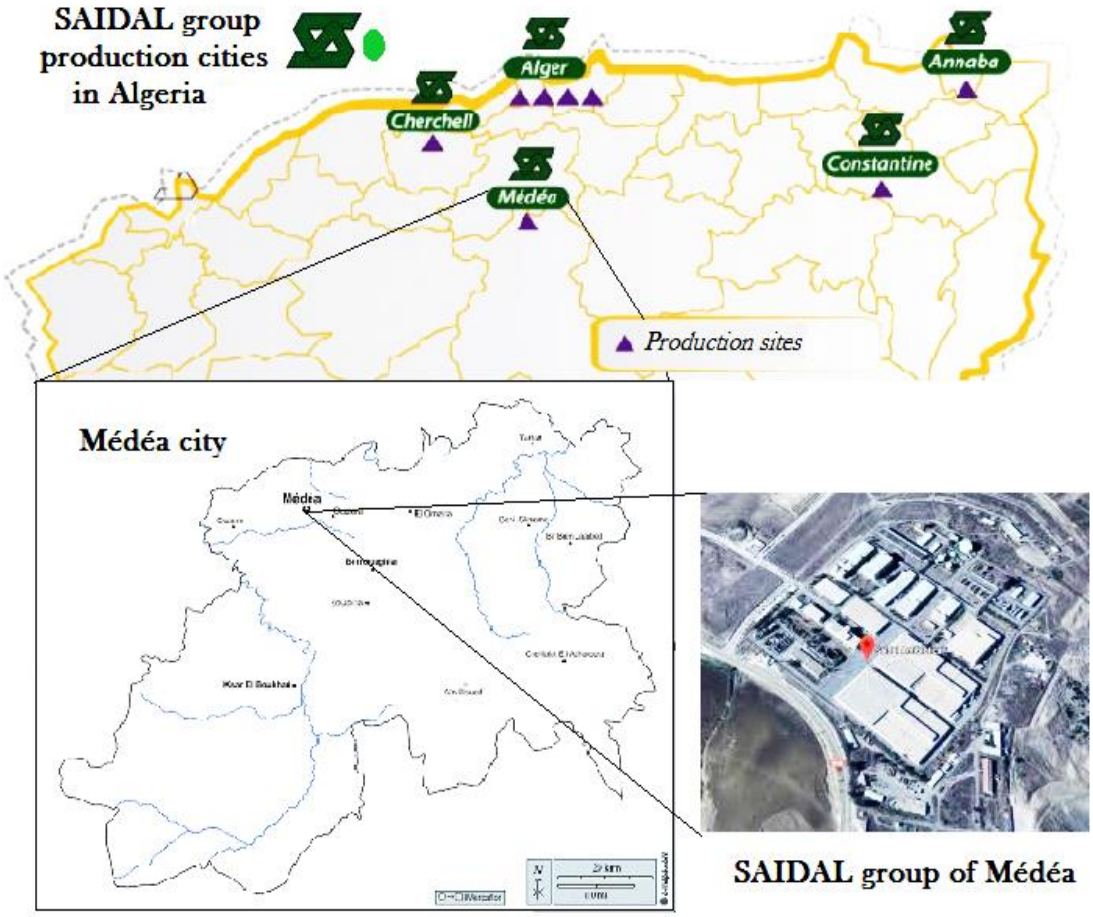

Figure 2 – Location of the sampling site of the SAIDAL group in Médéa.

The complex has an area of 25 hectares with 19 hectares of built area. The medéa antibiotic complex has several buildings and annexes including (www.saidalgroup.dz):

- A bulk raw material production building by fermentation.
- A production building of bulk raw materials by chemical synook from fermentation products.
- Two building vessels of pharmaceutical specialties, one dedicated to penicillinic products and the other to non-penicillinic products.
- A unit of production of packaging articles (printing).

- General services were necessary for the operation of these facilities.

The wastewater collected was homogenized and combined with concentrated H_2SO_4 (2 mL / L) and kept in a refrigerator at 4 °C to avoid photo-catalyzed alteration **(Singh and Kumar, 2020b)**.

Table 2 provides a summary of the physical and chemical properties of the wastewater. It can be seen that the wastewater is complex with many components.

Table 2 – Characteristics of wastewater.

Parameters	Values	Unit
potential Hydrogen	7.54±0.09	-
Turbidity	44.92±0.06	NTU
UV 254	0.353±0.01	-
DOC	18.50±0.04	mg/L
Conductivity	1968.00±0.17	µS cm^{-1}
Total dissolved solids	462.00±0.20	-
Nitrate	23.00±0.80	mg/L
Hardness	145.00±0.50	°F
Calcium	104.21±0.90	mg/L
Magnesium	136.45±0.60	mg/L
Total alkalimetric titre	283.50±0.30	mg/L
Bicarbonate	301.45±0.80	mg/L
Chlorides	342.54±0.40	mg/L
Nitrogen dioxide	0.10±0.07	mg/L
Ammonium	0.20±0.09	mg/L
Phosphate	0.20±0.02	mg/L
Sulfate	341.00±0.50	mg/L
Sodium	223.00±0.70	mg/L
Potassium	3.20±0.04	mg/L

Manganese	0.49±0.02	mg/L
Iron	1.50±0.06	mg/L
Aluminum	0.60±0.09	mg/L
Dry residues	1905.00±0.10	mg/L

2.2. RSM

According to Khuri and Cornell (1996), the RSM principle combines mathematical and statistical approaches for analyzing the connections between independent variables and one or more responses (Rifi et al., 2022; Tahraoui et al., 2021b). The design of experiment is required to get appropriate and reliable measurements of the responses that are of particular interest. A linear function cannot adequately reflect the connection between the response and the independent factors (Rifi et al., 2022; Singh and Kumar, 2020b). The use of a model that includes curvature is often required to estimate the response in the area near to ideal, and in most circumstances, a second-order model is sufficient to do this (Daud et al., 2018; Tahraoui et al., 2021b). A CCD is explored in detail, and it is a particularly effective design strategy for fitting second-order models that have been shown in (Rifi et al., 2022; Tahraoui et al., 2021b). This method is often employed when the output is influenced by various input elements (Rifi et al., 2022; Tahraoui et al., 2021b).

In conjunction with the CCD technique, the RSM approach is used to optimize the process under investigation. In this case, the independent factors considered are pH and the dosage of the coagulant, whereas DOC, UV 254, and turbidity are chosen as the dependent variables. The JMP program (version 13 pro) is used to perform the statistical analysis. The range of independent variables for the two coagulants ($CuSO_4$+ $FeCl_3$), and the combination relative to each other with a ratio (1:1, v/v), were chosen based on preliminary studies conducted to determine the amount of DOC reduced by each coagulant. Initial studies were conducted at pH values ranging from 2 to 13 (note that sodium hydroxide

(NaOH) and hydrochloric acid (HCl) were used for pH adjustment), and dosage levels ranging from 100 to 1500 mg / L. The parameters interval (pH and coagulant dosage) for both kinds of coagulants and the combination were determined based on the DOC decrease, as indicated in Table 3.

Table 3 – Coding and real levels for the CCD model.

Coagulant-floculant	pH (x1)			Coagulant-floculant mg/L(x2)		
	-1	0	+1	-1	0	+1
$CuSO_4$	7	9	11	600	900	1200
$FeCl_3$	3	5	7	200	600	1000
$CuSO_4 + FeCl_3$	5	7	9	200	600	1000

The complete factorial design CCD gives 13 experiments for each coagulant according to equation 1 (Tahraoui et al., 2021b) :

$$N = 2^k + 2k + c \quad (1)$$

where k is the number of independent variables, 2^k is the point factor, $2k$ is the axial points, and c is the number of experiments in the center points (Tahraoui et al., 2021b).

Once the range of independent variables for each incorporated coagulant and the set of different conditions have been obtained, the laboratory tests are carried out using the jar test, and the experimental results are incorporated into JMP shown in Table 4.

The jar test was carried out using beakers filled with 1 L of the collected effluent. Following the addition of the coagulant and pH adjustment by sodium hydroxide (NaOH) or hydrochloric acid (HCl) using pH meter type JP selecta , the samples were mixed at 180 rpm for 5 minutes to establish a homogeneous mixture and brought into contact between the pharmaceutical effluents and the coagulant, in order to neutralize the charge of the particles and to initiate the flocculation process by the formation of microflocs (Daud et al.,

2015; Khouni et al., 2020; Momeni et al., 2018; Verma et al., 2010). Following that, the speed was dropped to 40 rpm for 30 minutes to ensure the contacting and growth of the flocs (Daud et al., 2018; Momeni et al., 2018; Tahraoui et al., 2021b; Verma et al., 2010). Where, all experiments were conducted at a temperature of 18 ± 2°C. In addition, the time and mixing speed have been set with an automatic controller.

In each pot, the supernatant was taken after 45 minutes of decantation and filtered through pleated filter paper to determine the concentrations of DOC, UV 254, and turbidity. Conventional methods were used to perform the physicochemical analyzes. The turbidity and UV absorbance at 254 nm were measured, respectively, using a Hach 2100-year orchids turbidimeter and a Cecil Server 2 Gratin Spectrophotometer UV spectrophotometer. The water DOC dosage was carried out by the determination of potassium permanganate oxidizing (Fatombi et al., 2007; Rodier et al., 2016).

It should be noted that the DOC and UV 254 parameters are selected in this work due to the presence of the most used natural organic material (NOM) being the total organic carbon (COT) or the dissolved organic carbon (DOC), and Ultraviolet absorbance at a specific length, 254nm (UV 254) (HARRAT, 2013). These two parameters (DOC and UV 254) complement each other: the DOC provides indications on the quantity of NOM present and available for reaction, and UV 254 rather indicates its responsiveness since it is an indicator of the aromatic links contained in humic substances (HARRAT, 2013). Thus they can characterize conjugated systems (aromatic nuclei in particular), which are very abundant in the macromolecular structures that constitute the organic matter dissolved in natural waters (HARRAT, 2013).

2.3. Gaussian Process Rregression

Gaussian Process (GP) is a stochastic process with a series of random variables. Any finite range of those random variables has a joint Gaussian distribution. The probabilistic

illustration of a goal function can be used for regression and classification (Tahraoui et al., 2022b).

Gaussian Process Regression (GPR) provides a probabilistic, nonparametric strategy for solving nonlinear regression problems. GPR assumes that the measurements of the output variable *y* are generated in the following way (Park et al., 2017):

$$y = f\left(x(k)\right) + \varepsilon \quad (2)$$

where x stands for the measurements of input variables, f is the unknown functional dependence, and ε is a Gaussian noise with zero mean and variance σ_n^2. GPR uses GP as a prior to describe the distribution on the target function $f\left(x\right)$ (Park et al., 2017; Tahraoui et al., 2022b). In GPR, the function values $f_{1:n} = \left(f_1, ..., f_n\right)$ corresponding to the input values $x_{1:n} = \left(x_1, ..., x_n\right)$ are treated as random variables, where $f_i = f\left(x_i\right)$ (Park et al., 2017; Tahraoui et al., 2022b). GP is defined as a collection of random variables (stochastic process) and any finite number of which are assumed to be jointly Gaussian distributed (Park et al., 2017; Tahraoui et al., 2022b). GP can fully describe the distribution over an unknown function, $f\left(x\right)$, by its mean function, $m\left(x\right) = E\left[f\left(x\right)\right]$, and a kernel function, $k\left(x, x'\right)$, that approximates the covariance $E\left[\left(f\left(x\right) - m\left(x\right)\right)\left(f\left(x'\right) - m\left(x'\right)\right)\right]$. The kernel (covariance) function represents a geometrical distance measure assuming that the more closely located inputs would be more correlated in terms of their function values (Park et al., 2017; Tahraoui et al., 2022b). That is, the prior on the function values is represented as (Park et al., 2017; Tahraoui et al., 2022b):

$$\left(f^{1:n}\right) = GP\left(m(\cdot), k(\cdot,\cdot)\right)$$

(3)

where:

$m(.)$ is a mean function capturing the overall trend in the target function value and $k(.,.)$ is a kernel function used to approximate the covariance.

In GPR, the kernel (covariance) function describes the structure of the target function. Thus, the type of kernel function $k(x, x')$ used to build a GPR model and its parameters can strongly affect the overall representability of the GPR model and impact the accuracy of the prediction model. A wide variety of kernel functions can be used (Rasmussen and Williams, 2006).

In this article, the main objective is to create general models to predict the reduction rates of each dependent parameter for the three treatments using GPR. The dragonfly algorithm (DA) is used to optimize the GPR models by finding the best parameters of the karnel functions leading to the best performance. In this study, ten kernel functions have been optimized with Basis Function (constant, linear and zero) for each output and the one giving the best performance is selected.

The following ten karnel functions are used in this work:

- **Squared Exponential Kernel**

$$k\left(x_i, x_j \middle| \theta\right) = \sigma_f^2 \exp\left[-\frac{1}{2}\frac{\left(x_i - x_j\right)^T\left(x_i - x_j\right)}{\sigma_l^2}\right]$$

(4)

Where σ_l is the characteristic length scale, and σ_f is the signal standard deviation.

- **Exponential Kernel**

$$k\left(x_i, x_j \middle| \theta\right) = \sigma_f^2 \exp\left[-\frac{r}{\sigma_l}\right]$$

(5)

Where σ_l is the characteristic length scale and $r = \sqrt{\left(x_i - x_j\right)^T \left(x_i - x_j\right)}$

- **Matern 3/2**

$$k\left(x_i, x_j \middle| \theta\right) = \sigma_f^2 \left(1 + \frac{\sqrt{3}r}{\sigma_l}\right) \exp\left(-\frac{\sqrt{3}r}{\sigma_l}\right) \qquad \text{where } r = \sqrt{\left(x_i - x_j\right)^T \left(x_i - x_j\right)}$$

(6)

- **Matern 5/2**

$$k\left(x_i, x_j \middle| \theta\right) = \sigma_f^2 \left(1 + \frac{\sqrt{5}r}{\sigma_l} + \frac{5r^2}{3\sigma_f^2}\right) \exp\left(-\frac{\sqrt{5}r}{\sigma_l}\right) \qquad \text{where } r = \sqrt{\left(x_i - x_j\right)^T \left(x_i - x_j\right)}$$

(7)

- **Rational Quadratic Kernel**

$$k\left(x_i, x_j \middle| \theta\right) = \sigma_f^2 \left(1 + \frac{r^2}{2\alpha\sigma_l^2}\right)^{-\alpha}$$

(8)

Where σ_l is the characteristic length scale, α is a positive scale mixture parameter, and $r = \sqrt{\left(x_i - x_j\right)^T \left(x_i - x_j\right)}$.

- **ARD Squared Exponential Kernel**

$$k\left(x_i, x_j \middle| \theta\right) = \sigma_f^2 \exp\left[-\frac{1}{2}\sum_{m=1}^{d}\frac{\left(x_{im} - x_{jm}\right)^2}{\sigma_m^2}\right] \tag{9}$$

- **ARD Exponential Kernel**

$$k\left(x_i, x_j \middle| \theta\right) = \sigma_f^2 \exp\left(-r\right) \quad \text{where} \quad r = \sqrt{\sum_{m=1}^{d}\frac{\left(x_{im} - x_{jm}\right)^2}{\sigma_m^2}} \tag{10}$$

- **ARD Matern 3/2**

$$k\left(x_i, x_j \middle| \theta\right) = \sigma_f^2 \left(1 + \sqrt{3}r\right)\exp\left(-\sqrt{3}r\right) \quad \text{where} \quad r = \sqrt{\sum_{m=1}^{d}\frac{\left(x_{im} - x_{jm}\right)^2}{\sigma_m^2}} \tag{11}$$

- **ARD Matern 5/2**

$$k\left(x_i, x_j \middle| \theta\right) = \sigma_f^2 \left(1 + \sqrt{5}r + \frac{5}{3}r^2\right)\exp\left(-\sqrt{5}r\right) \quad \text{Where } r = \sqrt{\sum_{m=1}^{d}\frac{\left(x_{im} - x_{jm}\right)^2}{\sigma_m^2}} \tag{12}$$

- **ARD Rational Quadratic Kernel**

$$k\left(x_i, x_j \middle| \theta\right) = \sigma_f^2 \left(1 + \frac{1}{2\alpha} \sum_{m=1}^{d} \frac{\left(x_{im} - x_{jm}\right)^2}{\sigma_m^2}\right)^{-\alpha}$$

(13)

2.4. Statistical evaluation criteria

Statistic analysis and the ANOVA have been used to investigate the statistical abilities of the generated models with a confidence level of 95%. The statistical adequacy of the developed models was assessed using a variety of variables, including the P-value, the value F, the degree of freedom (DF), the coefficient of determination (R^2), the adjusted determination of the coefficient (R_{adj}^2), and the Root Mean Square Error (RMSE) (Tahraoui et al., 2021b, 2022b, 2022a). The value F describes the variation of the responses, which can be checked by a regression equation, while the value P determines the statistical adequacy of the developed model. For a model to be significant, the P-value must be less than 5%, and the P-value for the inadequacy test must be greater than 5% (Singh and Kumar, 2020b).

On the other hand, the Correlation Coefficient (R), R^2, R_{adj}^2, RMSE, Mean Square Error (MSE) and Mean Absolute Error (MAE), Error Standard of Prediction (ESP), Error Prediction of Model (EPM) were used to evaluate the performance of each GPR model. These are calculated using the following equations (Belsley et al., 1980; Bousselma et al., 2021; Hong et al., 2007; Tahraoui et al., 2022b, 2022a, 2021a, 2021b, 2020).

$$R = \frac{\sum_{i=1}^{N} \left(y_{\exp} - \bar{y}_{\exp}\right)\left(y_{pred} - \bar{y}_{pred}\right)}{\sqrt{\sum_{i=1}^{N} \left(y_{\exp} - \bar{y}_{\exp}\right)^2 \sum_{i=1}^{N} \left(y_{pred} - \bar{y}_{pred}\right)^2}} \quad (14)$$

$$R_{adj}^2 = 1 - \frac{\left(1 - R^2\right)\left(N - 1\right)}{N - K - 1} \quad (15)$$

$$RMSE = \sqrt{\left(\frac{1}{N}\right)\left(\sum_{i=1}^{N}\left[\left(y_{\exp} - y_{pred}\right)\right]^2\right)}$$

(16 $$MSE = \left(\frac{1}{N}\right)\left(\sum_{i=1}^{N}\left(y_{\exp} - y_{pred}\right)^2\right)$$

(17) $$MAE = \left(\frac{1}{N}\right)\sum_{i=1}^{N}\left|y_{\exp} - y_{pred}\right|$$

(18)

$$ESP(\%) = \frac{RMSE}{\overline{y}_{\exp}} \times 100$$

(19)

$$EPM(\%) = \frac{100}{N}\sum_{i=1}^{N}\left|\frac{\left(y_{\exp} - y_{\text{pred}}\right)}{y_{\exp}}\right|$$

(20)

Where N is the number of data samples, K is the number of variables (inputs), $y_{\exp}$ and y_{pred} are the experimental and the predicted values respectively, $\bar{y}_{\exp}$ and $\bar{y}_{pred}$ are respectively the average values of the experimental and the predicted values (Dolling and Varas, 2002; Manssouri et al., 2014, 2011).

3. Results and discussions

3.1. RSM

A statistical analysis of the developed RSM models was carried out using the "JMP 13 pro" program. This method found the mathematical relationship (Eq (3)) between two input parameters (pH and dosage) and three output parameters (DOC, UV 254, and turbidity) for three types of coagulants: $CuSO_4$, $FeCl_3$, and their mixture $CuSO_4$+ $FeCl_3$.

The results of 13 laboratory tests for the individual coagulants and their mixture are provided in Table 4, where the best experimental values are highlighted in bold and

underlined. It should be noted that the output parameters (DOC, UV 254 and turbidity) were predicted by their final concentrations. Subsequently, the final values of each parameter were converted into percentages by equation (21), in order to know the elimination rate of each output according to the coagulants/flocculants.

$$\text{Reduction rate (\%)}=\left(\frac{Z_i - Z_f}{Z_i}\right)\times 100 \quad (21)$$

Where Z_i is the initial value of each output (Table 2), and Z_f is the final value of each output.

Table 5 gives the statistical results necessary for the construction and interpretation of the RSM model. The equation took into account the two independent variables, the interactions between them, and their quadratic effect is given by Eq(21).

$$Y = \beta_0 + \beta_1 X_1 + \beta_2 X_2 + \beta_3 X_1 X_2 + \beta_4 X_1^2 + \beta_5 X_2^2 \quad (21)$$

where X_1 is pH, X_2 is dosage, Y is the response variable, β_0 to β_5 are the model parameters. Subsequently, the parameters with high explanatory power were retained (PR <5%) which are bolded and underlined in Table 5 (Tahraoui et al., 2021b), On the other hand, the other parameters which have PR >5% were deleted (which are in bold and underlined in Table 5), and the models are represented by the equations given in Table 6.

In the DOC model, the pH quadratic effect with the dose of $CuSO_4$ has proven to be a non-significant parameter as p = 12.32% and the same for the mixture dose ($CuSO_4$+FeCl) because their P = 20.82% (Table 5.a). In the UV 254 model, it is shown that the interaction between pH and the dose of $CuSO_4$ is not significant as p=10.23% (Table 5.b).

Finally, in the turbidity model, it is found that the pH interaction with the dose of $CuSO_4$ is non-significant parameter as p = 13.58% (Table 5.c). On the other hand, it is also found that the quadratic effect of the dose of $FeCl_3$ are insignificant parameters as p = 10.82% (Table 5.c).

Table 4 – Set of experimental conditions of independent variables (pH and dosage) and response (DOC, UV 254, and turbidity) for $CuSO_4$, $FeCl_3$ and $CuSO_4$+$FeCl_3$ coagulants.

Run. No	**$CuSo_4$**							
	Independente variables		Responses					
	pH	Dosage	DOC (mg/L)	DOC Reduction (%)	UV 254	UV 254 reduction (%)	Turbidity (NTU)	Turbidity reduction (%)
1	-1	-1	8.50±0.09	54.04±0.47	0.125±0.002	64.49±0.433	20.91±0.020	53.45±0.045
2	-1	0	6.50±0.10	64.86±0.54	0.115±0.003	67.51±0.911	18.80±0.180	58.16±0.401
3	-1	1	5.50±0.13	70.29±0.69	0.115±0.004	67.51±1.073	17.39±0.095	61.29±0.212
4	0	-1	4.50±0.05	75.68±0.27	0.113±0.002	67.89±0.433	15.07±0.105	66.46±0.234
5	0	0	4.00±0.10	78.38±0.54	0.104±0.004	70.63±0.995	13.34±0.025	70.31±0.056
6	0	0	4.00±0.08	78.36±0.42	0.105±0.003	70.25±0.850	13.38±0.053	70.21±0.118
7	0	0	4.00±0.03	78.40±0.14	0.104±0.001	70.44±0.164	13.38±0.074	70.21±0.164
8	0	0	4.00±0.07	78.40±0.35	0.106±0.005	70.06±1.397	13.25±0.066	70.50±0.146
9	0	0	4.00±0.12	78.38±0.62	0.106±0.004	70.06±1.179	13.3±0.045	70.38±0.100
10	0	1	4.10±0.09	77.84±0.46	0.110±0.006	68.83±1.700	12.47±0.042	72.25±0.093
11	1	-1	2.80±0.19	84.88±1.00	0.093±0.002	73.65±0.567	6.07±0.045	86.49±0.100
12	**1**	**0**	**1.78±0.11**	**90.38±0.59**	**0.080±0.001**	**77.71±0.327**	**2.46±0.045**	**94.52±0.100**

13	1	1	2.50±0.10	86.47±0.51	0.090±0.004	74.50±1.133	4.96±0.046	88.96±0.102
Run. No					**$FeCl_3$**			
	Independente variables				Responses			
	pH	Dosage	DOC (mg/L)	DOC Reduction (%)	UV 254	UV 254 reduction (%)	Turbidity (NTU)	Turbidity reduction (%)
1	-1	-1	5.60±0.18	69.75±0.949	0.112±0.006	68.27±1.769	11.09±0.123	75.30±0.275
2	-1	0	4.80±0.10	74.04±0.541	0.109±0.003	69.21±0.713	10.13±0.047	77.45±0.105
3	-1	1	4.40±0.06	76.22±0.337	0.101±0.004	71.38±1.133	9.58±0.410	78.66±0.913
4	0	-1	7.20±0.12	61.08±0.623	0.134±0.004	61.94±1.145	14.85±0.026	66.94±0.059
5	0	0	4.00±0.05	78.38±0.286	0.097±0.003	71.48±0.911	9.51±0.224	78.83±0.498
6	0	0	4.00±0.16	78.38±0.842	0.099±0.002	71.95±0.567	9.60±0.116	78.63±0.258
7	0	0	4.00±0.03	78.38±0.162	0.100±0.006	71.76±1.731	9.56±0.015	78.72±0.034
8	0	0	4.00±0.07	78.38±0.354	0.098±0.002	72.14±0.433	9.55±0.156	78.74±0.348
9	0	0	4.00±0.09	78.38±0.510	0.100±0.004	70.91±1.073	9.60±0.228	78.63±0.508
10	**0**	**1**	**2.50±0.17**	**86.49±0.922**	**0.093±0.004**	**73.56±0.495**	**4.46±0.040**	**90.07±0.090**
11	1	-1	12 .0±0.12	35.14±0.655	0.244±0.007	30.87±1.963	29.68±0.184	33.92±0.409
12	1	0	7.20±0.08	61.08±0.408	0.162±0.006	54.10±1.700	18.96±0.038	57.78±0.084
13	1	1	3.70±0.13	79.98±0.695	0.130±0.006	67.89±1.560	9.02±0.025	79.91±0.056
Run. No					**$CuSo_4$+$FeCl_3$**			
	Independente variables				Responses			
	pH	Dosa	DOC	DOC	UV 254	UV 254	Turbidit	Turbidit

		ge	(mg/L)	Reductio n (%)		reductio n (%)	y (NTU)	y reductio n (%)
1	-1	-1	1.70±0. 05	90.79±0. 24	0.110±0. 003	68.83±0. 850	3.60±0.1 01	91.98±0. 226
2	**-1**	**0**	**0.50±0. 03**	**97.32±0. 14**	**0.060±0. 002**	**82.90±0. 433**	**1.58±0.0 40**	**96.47±0. 090**
3	-1	1	3.00±0. 03	83.78±0. 14	0.130±0. 003	63.26±0. 865	6.20±0.1 10	86.20±0. 245
4	0	-1	2.90±0. 18	84.31±0. 95	0.153±0. 004	56.65±1. 235	5.58±0.0 17	87.57±0. 039
5	0	0	1.42±0. 35	92.34±0. 79	0.113±0. 005	68.08±1. 277	3.30±0.0 42	92.66±0. 093
6	0	0	1.48±0. 02	92.00±0. 09	0.114±0. 004	67.80±0. 995	3.20±0.0 96	92.86±0. 214
7	0	0	1.45±0. 14	92.18±0. 74	0.110±0. 004	68.74±1. 145	3.25±0.0 15	92.75±0. 034
8	0	0	1.40±0. 03	92.43±0. 16	0.112±0. 003	68.27±0. 981	3.30±0.0 10	92.65±0. 022
9	0	0	1.47±0. 03	92.05±0. 19	0.109±0. 004	69.12±1. 021	3.20±0.1 50	92.88±0. 335
10	0	1	1.60±0. 09	91.33±0. 46	0.115±0. 006	67.42±1. 769	3.70±0.0 74	91.75±0. 164
11	1	-1	3.50±0. 12	81.10±0. 65	0.165±0. 006	53.16±1. 731	7.18±0.0 30	84.01±0. 067
12	1	0	2.90±0. 03	84.31±0. 17	0.155±0. 004	56.09±1. 235	6.15±0.0 98	86.31±0. 218
13	1	1	2.60±0. 07	85.96±0. 38	0.150±0. 003	57.60±0. 713	5.50±0.1 95	87.75±0. 433

Table 5 shows the results of the RSM performance in terms of all errors as well as in terms of agreement vector values.

Table 5 – Results of the RSM

		$CuSo_4$				**$FeCl_3$**				**$CuSo_4$+$FeCl_3$**			
I	Term	*βi*	Std	*t*	Prob	*βi*	Std	*t* Ratio	Prob	*βi*	Std	*t*	Prob
						a. DOC							
0	Interc	3.946	0.12	30.7	4.48	4.05	0.06	58.88	1.06	1.41	0.048	28.97	1.501
1	X_1	-	0.12	-	0.00	1.35	0.06	19.92	2.00	0.41	0.048	8.663	5.460

2	X_2	-	0.12	-	0.00	-	0.06	-	4.09	**0.06**	**0.048**	**1.386**	**0.208**
3	X_1*X_2	0.675	0.15	4.37	0.00	-	0.08	-	1.23	-	0.058	-	0.000
4	X_1*X_1	**0.325**	**0.18**	**1.75**	**0.12**	1.79	0.09	17.96	4.08	-	0.070	-	0.003
5	X_2*X_2	0.485	0.18	2.61	0.03	0.64	0.09	6.455	0.00	1.54	0.070	21.86	1.057
						b. UV 254							
0	Interc	0.104	0.00	135.	3.15	0.09	0.00	30.82	9.76	0.11	0.002	53.41	1.373
1	X_1	-	0.00	-	1.84	0.03	0.00	11.26	9.71	0.02	0.002	10.66	2.971
2	X_2	-	0.00	-	0.00	-	0.00	-	5.17	**0.00**	**0.002**	**0.57**	**0.583**
3	X_1*X_2	**0.001**	**0.00**	**1.88**	**0.10**	-	0.00	-	0.00	-	0.002	-	5.287
4	X_1*X_1	-	0.00	-	0.00	0.03	0.00	7.506	0.00	-	0.002	-	4.041
5	X_2*X_2	0.007	0.00	6.55	0.00	0.01	0.00	2.792	0.02	0.04	0.001	15.59	3.864
						c. Turbidity							
0	Interc	13.15	0.29	44.3	7.77	9.53	0.07	133.3	3.51	3.19	0.080	39.97	1.595
1	X_1	-	0.29	-	4.29	4.47	0.07	63.68	6.18	0.83	0.078	10.59	1.463
2	X_2	-	0.29	-	0.00	-	0.07	-	1.61	0.24	0.078	3.155	0.016
3	X_1*X_2	**0.602**	**0.35**	**1.69**	**0.13**	-	0.08	-	1.59	-	0.096	-	1.069
4	X_1*X_1	-	0.43	-	0.00	5.08	0.10	49.03	3.83	-	0.115	-	0.007
5	X_2*X_2	1.049	0.43	2.44	0.04	**0.19**	**0.10**	**1.840**	**0.10**	2.79	0.115	24.06	5.440

Table 6 – RSM performances For $CuSO_4$, $FeCl_3$ and $CuSO_4$+$FeCl_3$ coagulant.

Responses	Final equation in terms of code of independent variables	P	F	R^2	R^2_{adj}	RMSE	DF
	$CuSO_4$						
DOC	$Y = 3.9468 - 2.2366X_1 - 0.6166X_2 + 0.675X_1X_2 + 0.4858X_2^2$	6.453 e-6	74.5665	0.9815	0.9684	0.3090	5
UV 254	$Y = 0.1047 - 0.0153X_1 - 0.0026X_2 - 0.0066X_1^2 + 0.0073X_2^2$	2.7291 e-6	95.8741	0.9856	0.9753	0.0018	5
Turbidity	$Y = 13.1558 - 7.2683X_1 - 1.205X_2 - 2.0905X_1^2 + 1.0494X_2^2$	8.8865 e-7	132.8157	0.9895	0.9821	0.7149	5
	$FeCl_3$						
DOC	$Y = 4.0586 + 1.35X_1 - 2.3666X_2 - 1.775X_1X_2 + 1.7948X_1^2 + 0.6448X_2^2$	7.7248 e-9	520.6865	0.9973	0.9954	0.1660	5
UV 254	$Y = 0.0992 + 0.0356X_1 - 0.0276X_2 - 0.0257X1X2 + 0.0350X_1^2 + 0.0130X_2^2$	8.7505 e-6	68.1960	0.9798	0.9655	0.0077	5
Turbidity	$Y = 9.5355 + 4.4766X_1 - 5.4266X_2 - 4.7875X_1X_2 + 5.0806X_1^2$	1.3553 e-11	3200.8552	0.9995	0.9992	0.1721	5

	$CuSO_4$+$FeCl_3$					
DOC	$Y = 1.4172 + 0.4166X_1 - 0.55X_1X_2 - 0.3003X_1^2 + 1.5496X_2^2$	**8.9978 e-7**	**132.3374**	**0.9895**	**0.9820**	**0.1178**	**5**
UV 254	$Y = 0.1103 + 0.0216X_1 - 0.0087X_1X_2 - 0.0198X_1^2 + 0.0466X_2^2$	**3.7414 e-9**	**640.9499**	**0.9978**	**0.9962**	**0.0026**	**5**
Turbidity	$Y = 3.1996 + 0.8333X_1 + 0.2483X_2 - 1.0700X_1X_2 - 0.4337X_1^2 + 2.7912X_2^2$	**3.6491 e-7**	**171.8152**	**0.9919**	**0.9861**	**0.1927**	**5**

The values of the coefficients of determination have decreased slightly, but the equation has become simpler after removing the low explanatory power variables. These coefficients mean that the correlations of the model were moderately positive (Figure 3). The probability was strictly below 0.5%, confirming that the model was significant (Tahraoui et al., 2021b).

The values of the significance level P and the values of the F Ratio, which provide a measure of the statistical significance of the regression models, have also been determined (Tahraoui et al., 2021b). A high value of F combined with a low value of P indicates that the equation is statistically significant (Tahraoui et al., 2021b).

1. $CuSO_4$

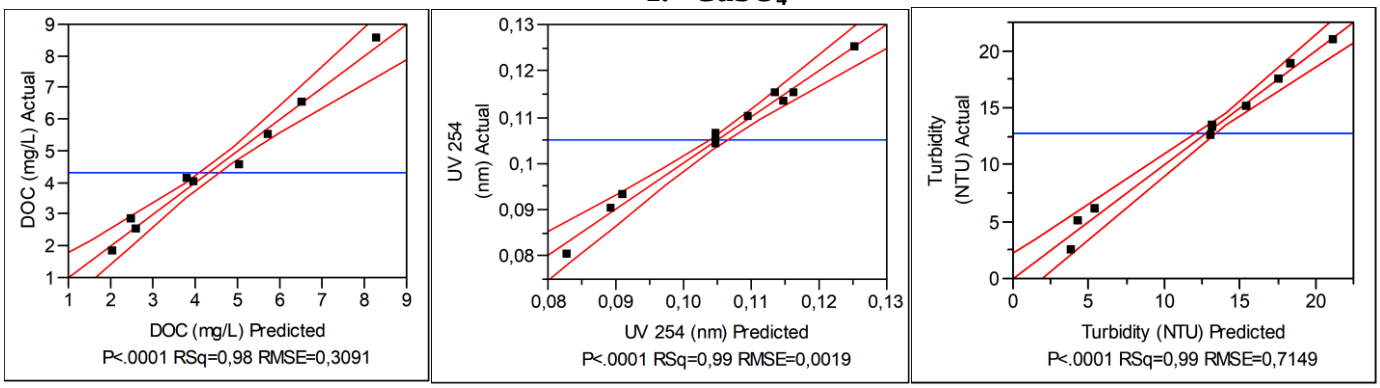

(a) **(b)** **(c)**

2. $FeCl_3$

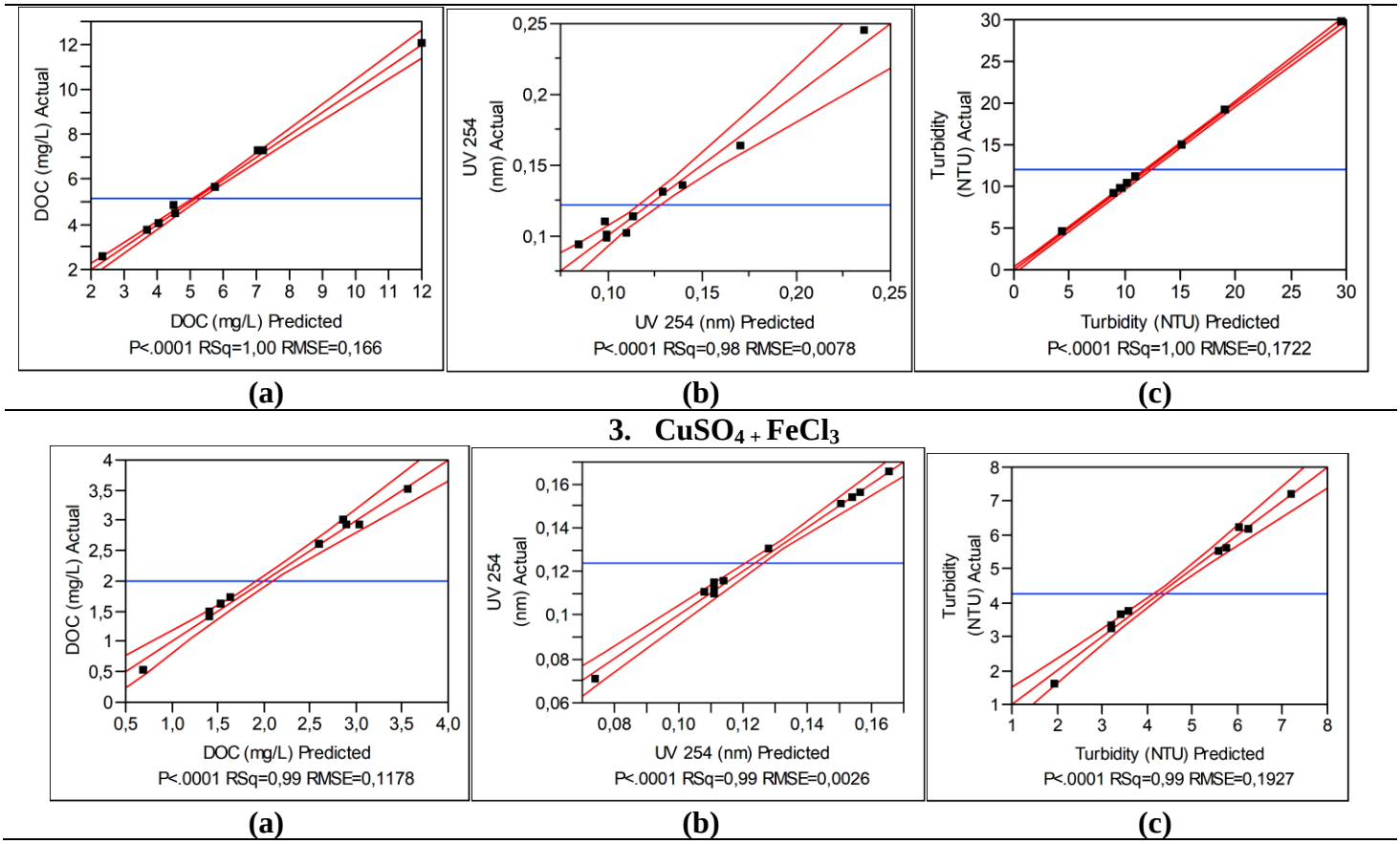

Figure 3 – Relation between the observed dose of coagulant and those estimated by the RSM model For $CuSO_4$, $FeCl_3$ and $CuSO_4$+$FeCl_3$ coagulants: (a) DOC, (b) UV 254, (c) Turbidity.

The proposed models can simultaneously infer the effect of the predictors (X_I and X_2), their interactions, and their quadratic effects. Table 5 shows the effects of independent factors, their interactions, and their quadratic terms on DOC, UV 254, and turbidity on the phenomenon of flexing coagulant. Indeed, the coefficients of each factor in the model make it possible to evaluate the impact of each factor on the answer (Lefnaoui and Moulai-Mostefa, 2014).

3.1.1. Effect of parameters on DOC

The pH factor is found to affect DOC positively under $FeCl_3$ and the mixture ($CuSO_4$ + $FeCl_3$) as shown in Table 5.a. On the other hand, it has a negative effect on DOC under

$CuSO_4$, i.e. each time the pH increases, the concentration of DOC decreases, as ahown in Table 5.a.

The dosage factor shows a negative effect on DOC under $CuSO_4$ and $FeCl_3$ as shown in Table 5.a. On the other hand, its effect on DOC is negligible under the mixture because it is an insignificant parameter as shown in Table 5.a.

On the other hand, Table 5.a shows that the interaction of pH and dosage has a positive effect on DOC under $CuSO_4$ and a negative effect on DOC under $FeCl_3$ and under the mixture ($CuSO_4$ + $FeCl_3$).

The pH has a negative quadratic effect on DOC in the presence of the mixture and a positive quadratic effect in the presence of $FeCl_3$ as shown in Table 5.a. However, its quadratic effect in the presence of $CuSO_4$ is considered negligible because prob>5% as shown in Table 4.a and Figure 5.a.

On the other hand, the dosage has positive quadratic effects in the presence of $CuSO_4$, $FeCl_3$ and the mixture as can be seen from Table 5.a.

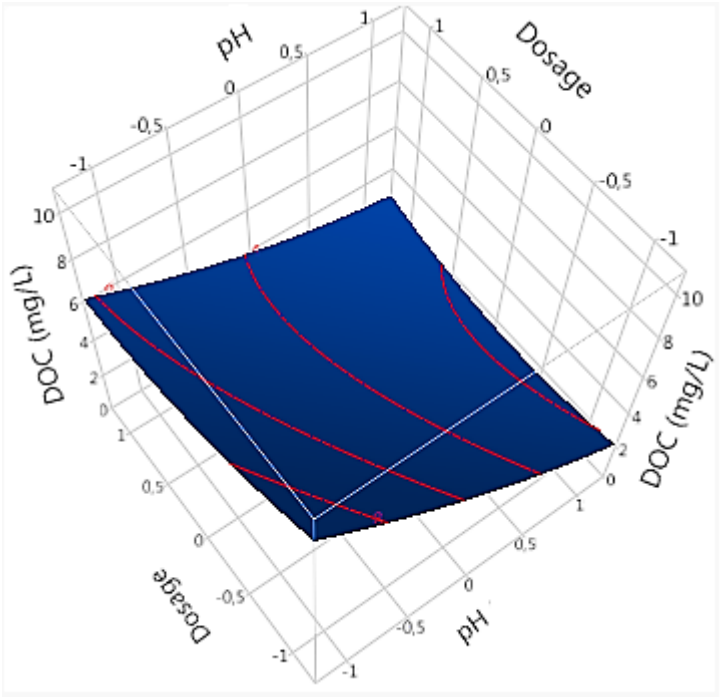

(a)

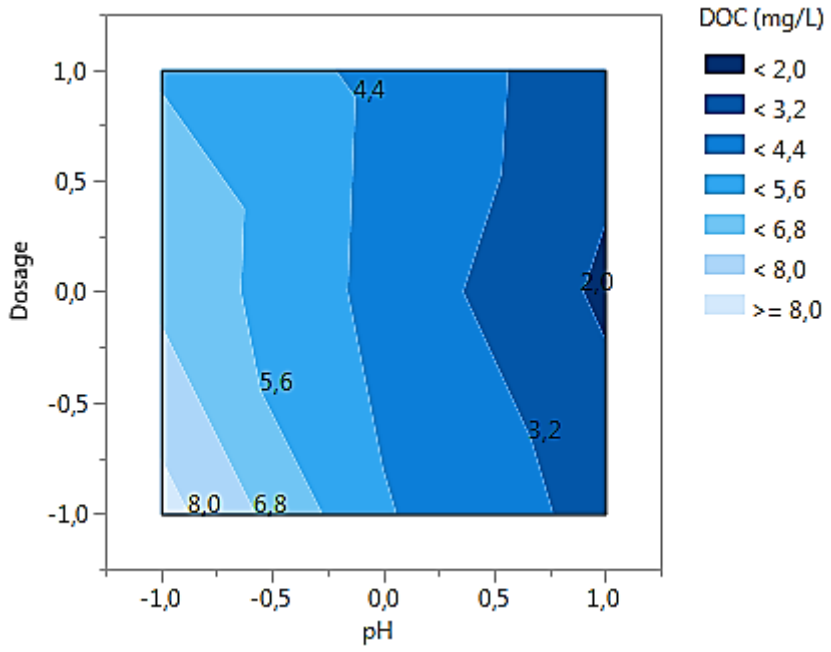

(b)

Figure 4 – Effects of operating factors and their interactions on DOC under $CuSO_4$: (a) interaction of coagulant dosage and pH, (b) contour plot.

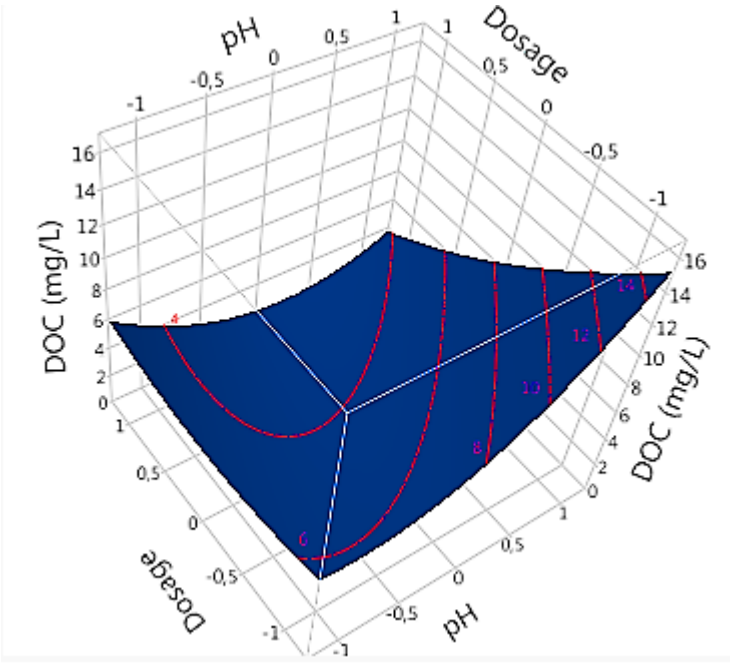

(a)

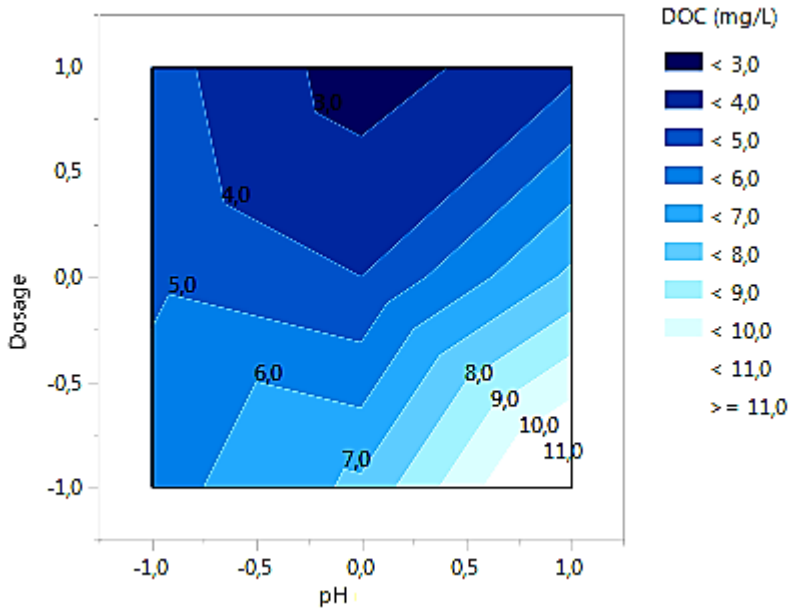

(b)

Figure 5 – Effects of operating factors and their interactions on DOC under $FeCl_3$: (a) interaction of coagulant dosage and pH, (b) contour plot.

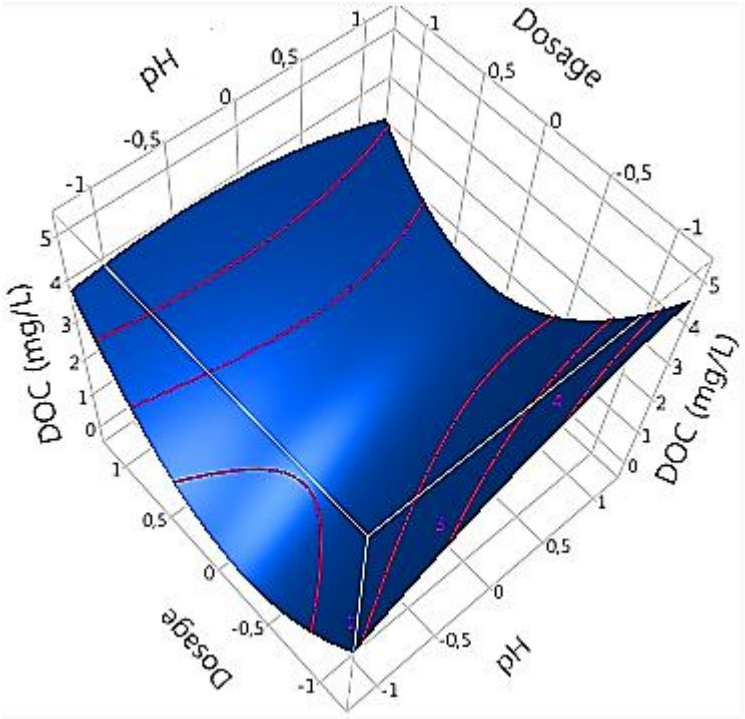

(a)

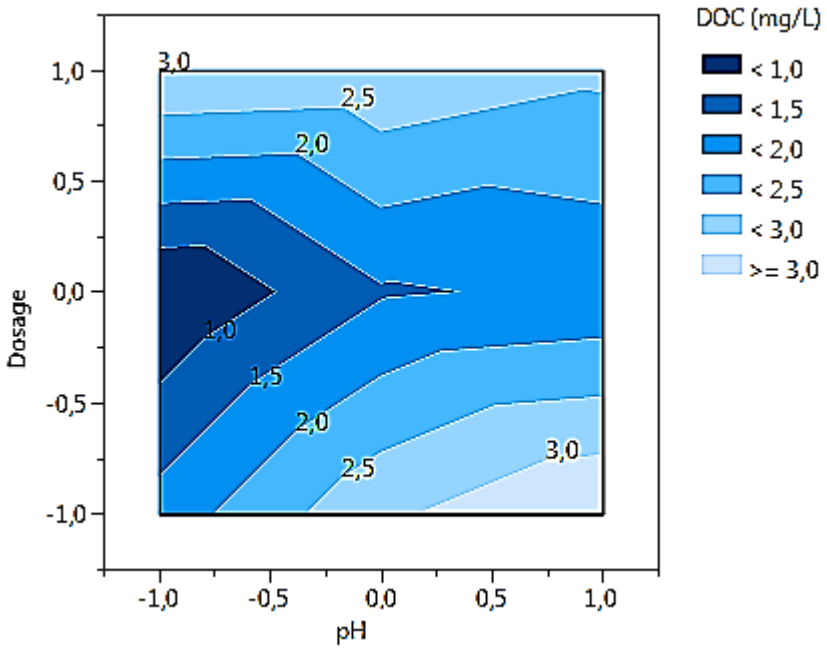

(b)

Figure 6 – Effects of operating factors and their interactions on DOC under $CuSO_4$ + $FeCl_3$: (a) interaction of coagulant dosage and pH, (b) contour plot.

From the obtained results shown in Figure 4.a, it appears that with increase in pH from 7 to 11, the DOC concentration decreases from 8.28 mg/L to 2.46 mg/L in the presence 600 mg/L of $CuSO_4$. Moreover, the pH has positive and negative quadratic effects on DOC in the presence of $FeCl_3$ and the mixture as shown in Figures 5 and 6 respectively. The concentration of DOC in the presence 1000 mg/L of $FeCl_3$ decreases from 4.55 mg/L to 2.33 mg/L for pH changing from 3 to 5 and then increases to 3.7 mg/L for pH=7 as shown in Figure 5.a. On the other hand, the concentration of DOC in the presence 1000 mg/L of the mixture increases from 2.86 to 3.04 mg/L for pH ranging from 5 to 5.875 and then decreases to 2.59 mg/L for pH = 9 as shown in Figure 6.a.

It should also be noted that the dosage of coagulant flocculant has a positive quadratic effect under $CuSO_4$, $FeCl_3$, and the mixture. The DOC concentration decreases from 2.43 to 2.01 mg/L for the $CuSO_4$ dosage changing from 600 to 900 mg/L at pH 11 and then

increases to 2.58 mg/L for the dosage equal to 1200 mg/L as shown in Figure 4.a. The DOC concentration decreases from 5.73 to 4.36 mg/L for the $FeCl_3$ dosage changing from 200 to 800 g/L at pH 3 and then increases to 4.55 mg/L at the dosage = 1000 mg/L as shown in Figure 5.a.

The DOC concentration decreases from 1.63 to 0. 63 mg/L for the mixture dose changing from 200 to 520 mg/L at pH 5 and then increases to 2.86 mg/L at dosage = 1000 mg/L as shown in Figure 6.a.

Very high DOC removal to 2.01, 2.31 and 0.63 mg/L provides a treatment efficiency equal to 89.13%, 86.48 and 97.27% respectively for $CuSO_4$, $FeCl_3$ and the mixture. The results in Figures 4 to 6 indicate the approximate optimal treatment condition are as follows: the pH must be adjusted and the coagulant-flocculant dosage injected according to $CuSO_4$, $FeCl_3$ and the mixture as follows: pH = 11, dosage = 900 mg/L (Figure 4.b); pH = 5, dosage = 1000 mg/L (Figure 5.b); pH = 5, dosage = 520 mg/L (Figure 6.b)).

From these results, it can be concluded that the coagulant-flocculant mixture ($CuSO_4$ + $FeCl_3$) removes DOC better than the individual coagulants. However, it should also be noted that the separate coagulants remain very practical according to the results obtained.

3.1.2. Effect of Parameters on UV 254

The pH factor is found to have a positive effect on UV 254 when using $FeCl_3$ and the mixture ($CuSO_4$ + $FeCl_3$) as shown in Table 5.b. On the other hand, it has a negative effect when $CuSO_4$ is used according to Table 5.b.

Moreover, the dosage factor shows a negative effect on UV 254 for $CuSO_4$ and $FeCl_3$ as shown in Table 5.b. However, it is considered as an insignificant parameter in presence of the mixture as shown in Table 5.b.

In contrast, the interaction of pH with dosage has a negative effect on UV 254 under $FeCl_3$ and the mixture ($CuSO_4$ + $FeCl_3$) according to Table 5.b. On the other hand, the effect of

the interaction of pH with the $CuSO_4$ dosage is negligible because it is an insignificant parameter (Table 5.b and Figure 7.a)

In addition, the results show that pH has a negative quadratic effect on UV 254 in the presence of $CuSO_4$ and mixture as shown in Figure 7, and a positive quadratic effect in the presence of $FeCl_3$ according to Figures 8 and 9. On the other hand, the dosages of $CuSO_4$, $FeCl_3$ and of the mixture shown positive quadratic effects as can be seen from Figures 7, 8 and 9.

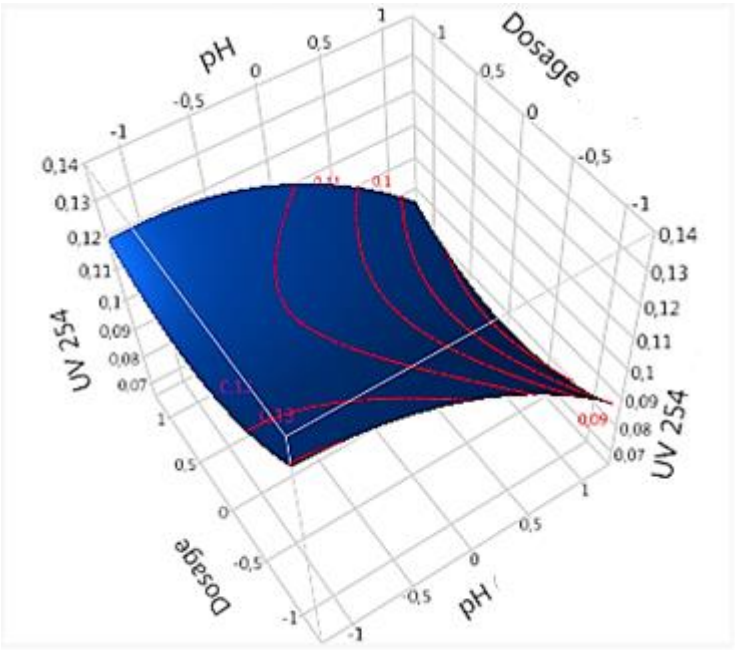

(a)

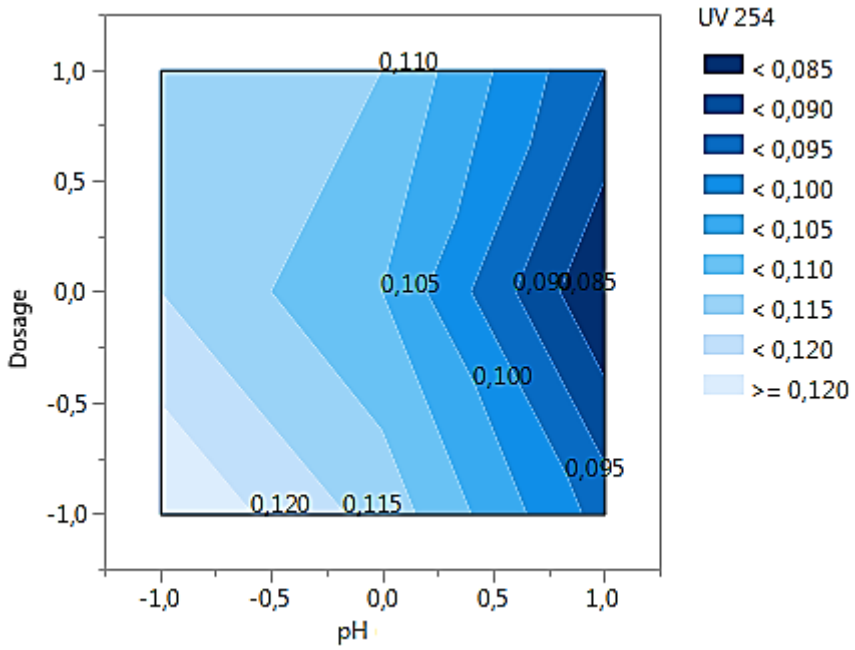

(b)

Figure 7 – Effects of operating factors and their interactions on UV 254 for $CuSO_4$:

(a) interaction of coagulant dosage and pH, (b) contour plot.

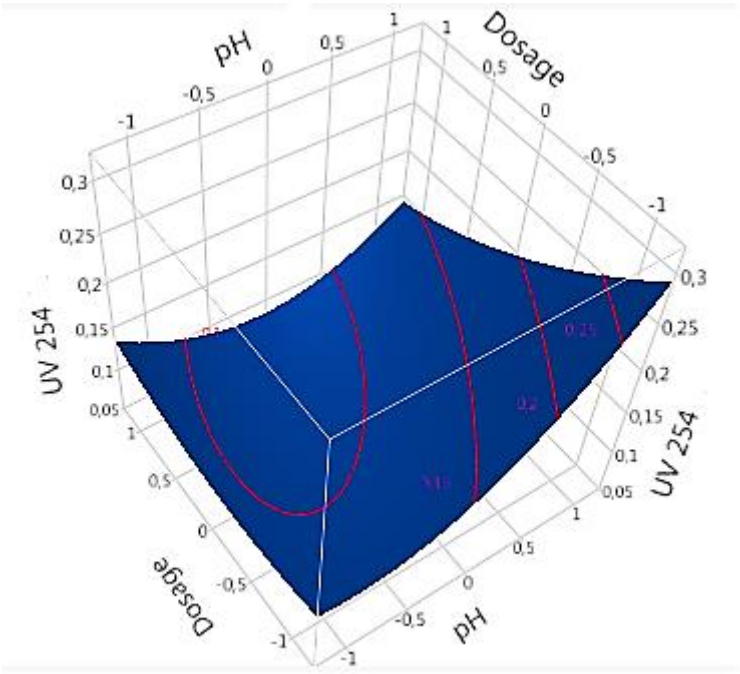

(a)

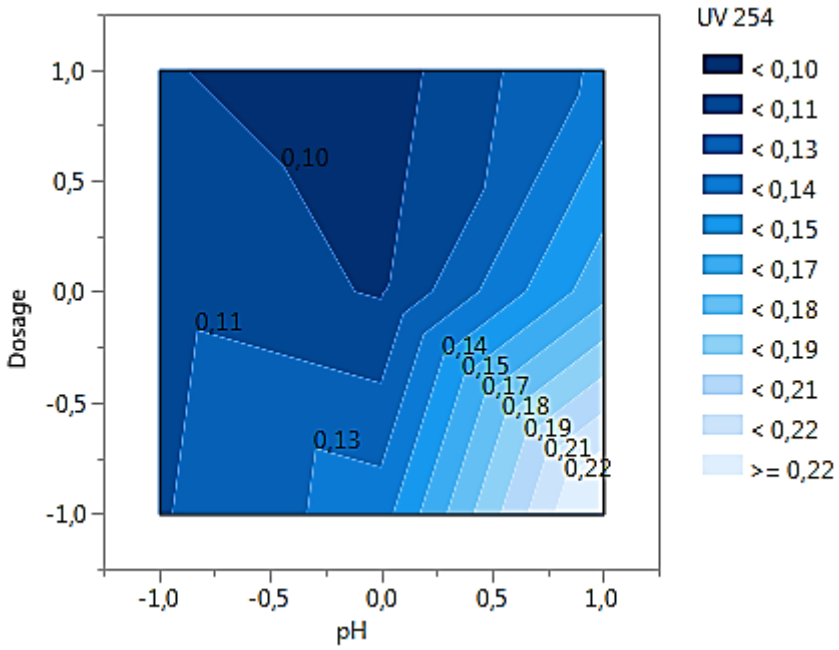

(b)

Figure 8 – Effects of operating factors and their interactions on UV 254 for $FeCl_3$: (a) interaction of coagulant dosage and pH, (b) contour plot.

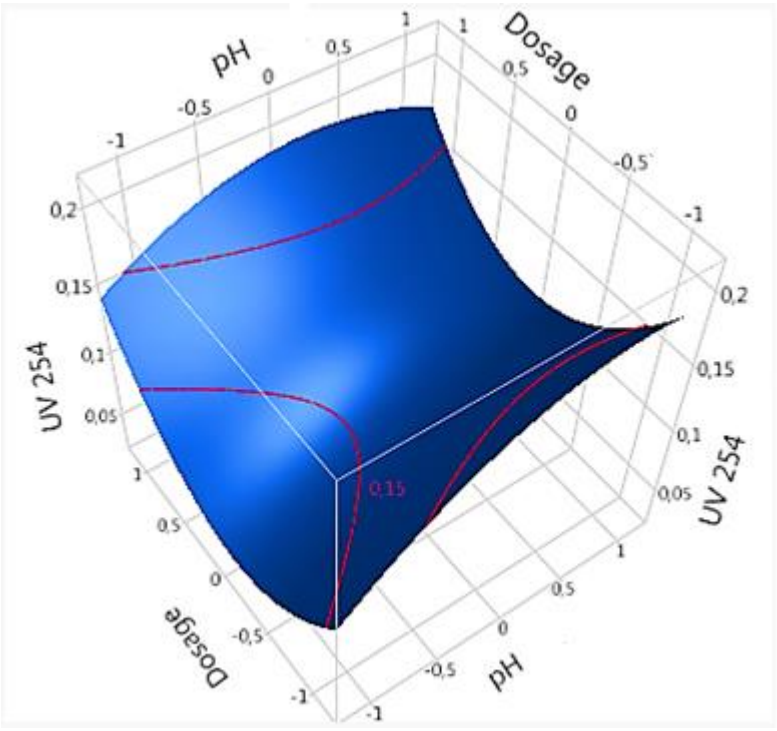

(a)

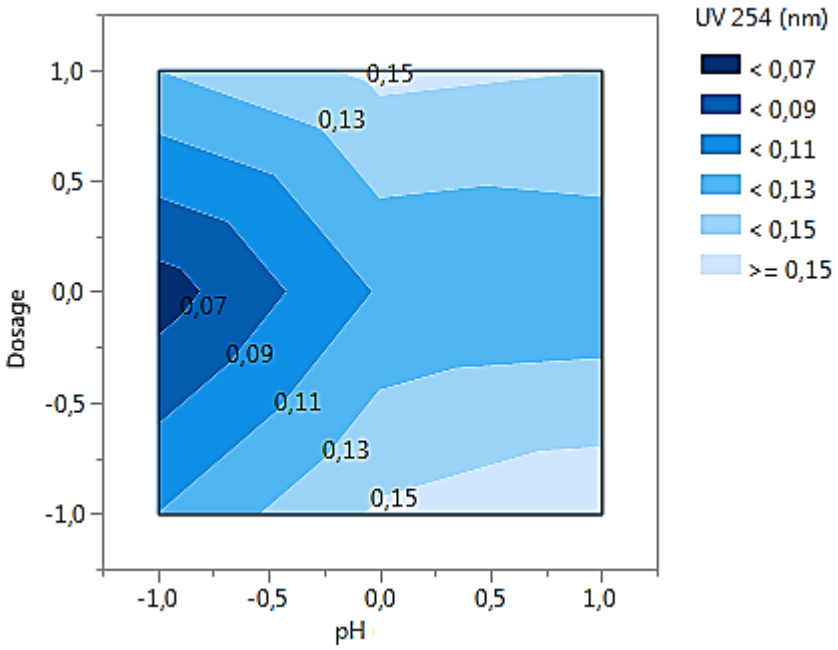

(b)

Figure 9 – Effects of operating factors and their interactions on UV 254 for $CuSO_4$ + $FeCl_3$: (a) interaction of coagulant dosage and pH, (b) contour plot.

Given the results obtained, it appears that the pH has a negative quadratic effect on UV 254 in the presence of $CuSO_4$ and the mixture, and a positive quadratic effect for $FeCl_3$. Indeed, the value of UV 254 in the presence 600 mg/L of $CuSO_4$ for a pH lower than 7 shows a positive effect, and for a pH change from 7 to 11, the value of UV 254 decreases from 0.125 to 0.091 (Figure 7. a). On the other hand, in the presence 1000 mg/L of $FeCl_3$, the value of UV 254 goes from 0.109 to 0.084 for a pH going from 3 to 5 then increases to 0.129 at pH = 7 (Figure 8.a). However, the UV value at 254 nm in the presence of 1000 mg/L of the mixture increases from 0.125 to 0.160 when the pH is increased from 5 to 7.64, then decreases again to 0.151 when the pH reaches 9 (Figure 9.a) .

On the other hand, coagulant flocculant dosage also has a positive quadratic effect on UV 254 under $CuSO_4$, $FeCl_3$ and mixture, as UV 254 value decreases from 0.090 to 0.082 for $CuSO_4$ dosage changes from 600 to 900 mg/L at pH = 11, then a slight increase (0.089) for

the dosage = 1200 mg/L (Figure 7.a). For $FeCl_3$, a slight decrease in the UV 254 value is observed from 0.113 to 0.098 for dosage going from 200 to 600 mg/L at pH = 3; as well as a slight increase up to the value 0.109 for the dosage equal to 1000 mg/L (Figure 8.a).

However, in the presence of mixture, the UV 254 value decreases from 0.105 to 0.068 corresponding to the dosage increases from 200 to 520 mg/L at pH 5; then increases to 0.125 for the dosage = 1000 mg/L (Figure 9.a).

In conclusion, having aromatic nucleus removal rates as UV absorbance at wavelength of 254 nm equal to 0.082, 0.084 and 0.068 or having a treatment efficiency equal to 76.77%, 76.20% and 80.73% using respectively $CuSO_4$, $FeCl_3$ and the mixture, the pH and the coagulant-flocculant dosage must be adjusted as follows: pH = 11, dosage = 900 mg/L (Figure 7.b); pH = 5, dosage = 1000 mg/L (Figure 8.b); pH = 5, dosage = 520 mg/L (Figure 9.b).

From these results, it can be concluded that the coagulant-flocculant mixture ($CuSO_4$ + $FeCl_3$) removes the aromatic rings better than the coagulants alone. However, it should also be noted that coagulants alone remain very effective in terms of the results obtained.

3.1.3. Effect of parameters on turbidity

The pH factor is found to have a positive effect on turbidity when $FeCl_3$ or the mixture is used as can be seen from Table 5.c. On the other hand, it has a negative effect on turbidity when $CuSO_4$ is used (Table 5.c). Moreover, the dosage factor shows a negative effect on turbidity when $CuSO_4$ or $FeCl_3$ is used and a positive effect when the mixture is used (Table 5.c).

The interaction of pH with dosage has a negative effect on turbidity under $FeCl_3$ or mixture (Table 5.c). On the other hand, the interaction of pH with the dosage in the presence of $CuSO_4$ is considered to have a negligible effect on turbidity because it is an insignificant parameter (Table 5.c and Figure 10.a).

Moreover, the results show that the dosage has a positive quadratic effect on the turbidity in the presence of $CuSO_4$ and the mixture (Table 5.c, Figures 10.a and 12.a), but the quadratic effect of $FeCl_3$ dosage on turbidity is negligible because it is an insignificant parameter (Table 5.c, Figure 11.a).

However, pH has interesting quadratic effects, indicating negative quadratic effects in the presence of CuSO4 and the mixture (Figures 10 and 12), but a positive effect in the presence of FeCl3 (Figure 11).

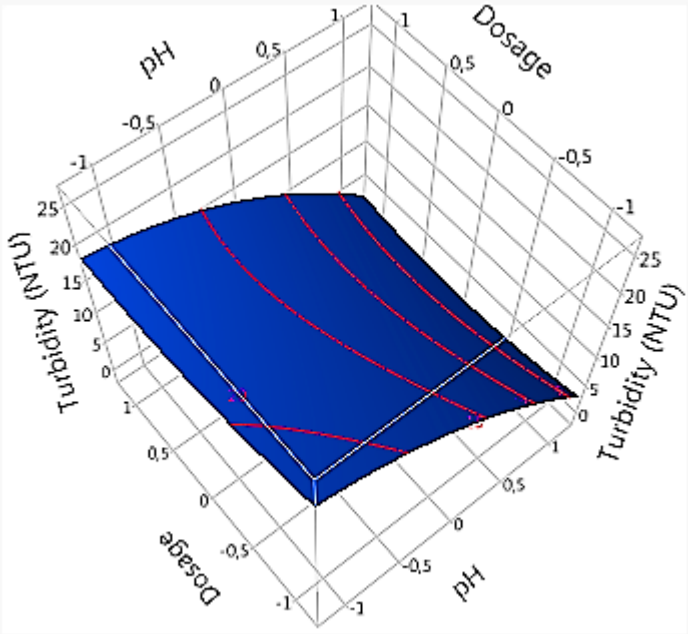

(a)

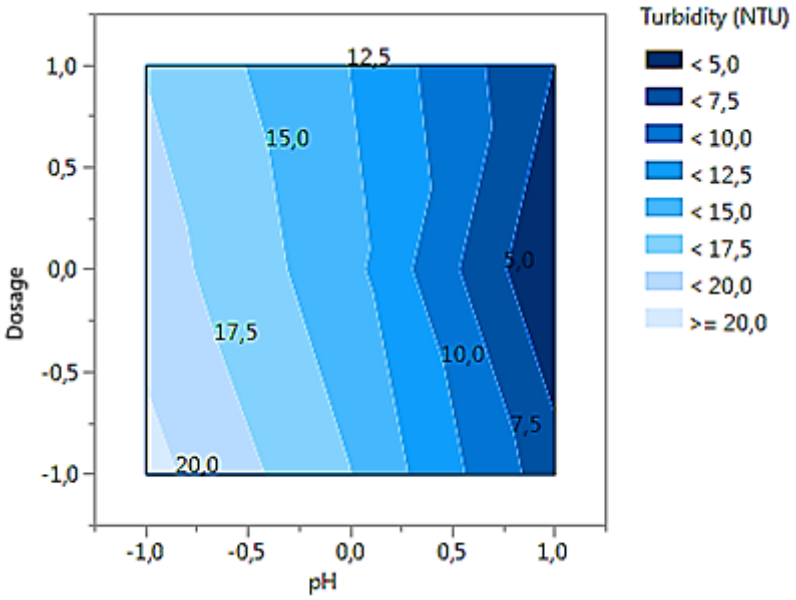

(b)

Figure 10 – Effects of operating factors and their interactions on turbidity for $CuSO_4$: (a) interaction of coagulant dosage and pH, (b) contour plot.

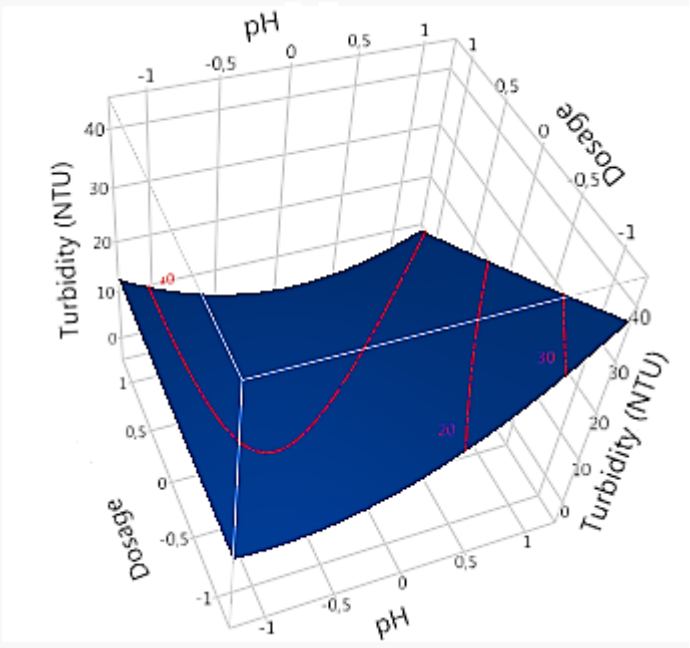

(a)

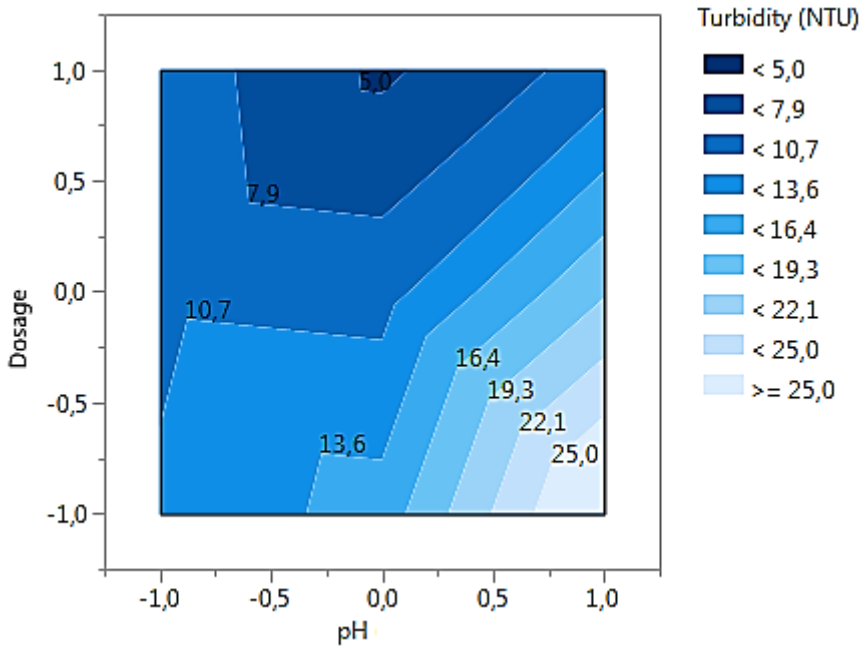

(b)

Figure 11 – Effects of operating factors and their interactions on turbidity for $FeCl_3$: (a) interaction of coagulant dosage and pH, (b) contour plot.

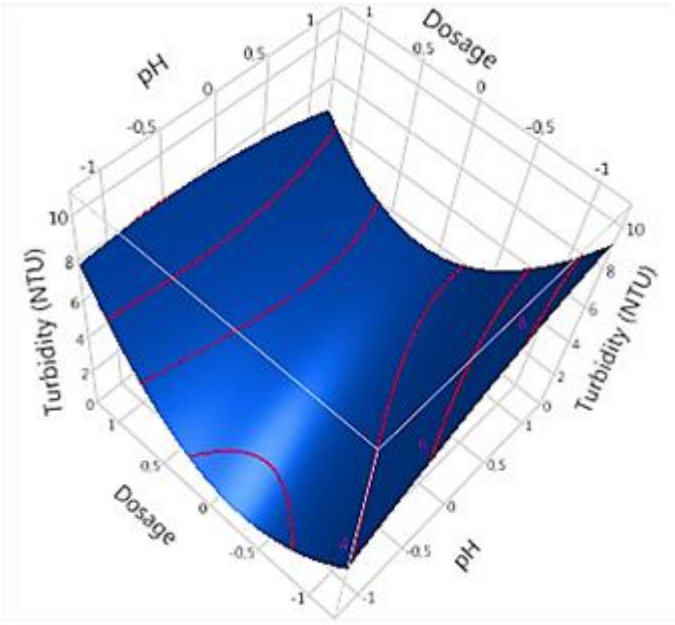

(a)

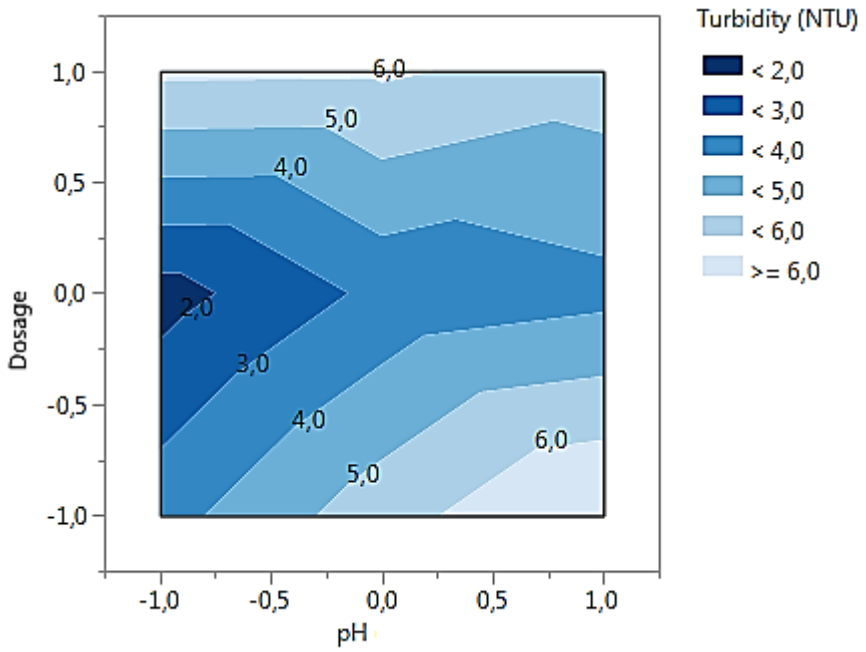

(b)

Figure 12 – Effects of operating factors and their interactions on turbidity $CuSO_4 + FeCl_3$: (a) interaction of coagulant dosage and pH, (b) contour plot.

Indeed, when pH is less than 7, it has a positive effect on turbidity in the presence 600 mg/L of $CuSO_4$, but when pH is increased from 7 to 11, turbidity decreases from 21.19 to 5.44 NTU (Figure 10.a).

With 1000 mg/L of $FeCl_3$, the turbidity decreases from 9.69 to 4.29 NTU when pH changes from 3 to 5 and increases to 9.06 NTU when pH=7 (Figure 11.a). On the other hand, the turbidity in the presence 1000 mg/L of the mixture increases from 6.04 to 6.23 NTU for pH changing from 5 to 7 and then decreases to 5.56 NTU when pH = 9 (Figure 12.a).

It should also be noted that the dosage of coagulant-flocculant has a positive quadratic effect only under $CuSO_4$ and the mixture (Figures 10, 11 and 12). For $CuSO_4$, a slight decrease in the turbidity value was observed from 5.32 to 3.57 NTU for a dosage ranging

from 600 to 900 mg/L when pH is at 11; as well as a slight increase up to the value 4.24 NTU for the dosage equal to 1200 mg/L (Figure 9.a). In the presence of the mixture, the turbidity decreases from 3.40 to 1.78 NTU for a dosage changing from 200 to 520 mg/L when pH is at 5, then increases to 6.04 NTU when the dosage is equal to 1000 mg/L (Figure 12.a).

For the dosage of $FeCl_3$, each time the dosage increases, the turbidity decreases. When increasing the dosage from 200 to 1000 mg/L, the turbidity is reduced from 10.96 to 9.06 NTU for $CuSO_4$ at pH = 3 (Figure 11.a).

For a turbidity removal rate equal to 3.57, 4.10 and 1.78 NTU or on condition of having a treatment efficiency equal to 91.56%, 90.44% and 96.05% in using $CuSO_4$, $FeCl_3$ and the mixture respectively, it is necessary to adjust the pH and inject the dosage of coagulant-flocculant according to $CuSO_4$, $FeCl_3$ and the mixture as follows: (pH = 11, dosage = 900 mg/L (Figure 10.b); pH = 5, dosage = 1000 mg/L(Figure 11.b); pH = 5, dosage = 520 mg/L(Figure 12.b)).

Therefore, it can be concluded that the coagulant-flocculant mixture ($CuSO_4$ + $FeCl_3$) removes turbidity better than the single coagulants. However, it should also be noted that the single coagulants remain very effective according to the results obtained.

3.2. GPR Modeling

The main goal of this part is to create more accurate models for the prediction of DOC, UV 254, and turbidity under the three treatments. For this, the databases of the first treatment ($CUSO_4$), the second treatment ($Fecl_3$), and the third treatment ($CuSo_4$+$Fecl_3$) were combined in a single database. In this database, a variable, "type of coagulation", has been inserted as a third independent parameter representing coagulation type, which was coded as 1, 2 and 3 for $CuSo_4$, $Fecl_3$ and $CuSo_4$+$Fecl_3$ respectively.

In order to develop more accurate models, the GPR was optimised by the dragonfly (DA) optimization algorithm to find the best appropriate parameters for Kernel Scale (SigmaM and SigmaF) and Sigma.

From the start, the database was split in two: 70% for learning and 30% for validation. the database has been normalized in the interval [-1,1] using the following equation:

$$x_N = 2\left(\frac{x - x_{\min}}{x_{\max} - x_{\min}}\right) - 1 \tag{22}$$

Then, as previously indicated, Ten kernel functions (exponential, exponential squared, mother32, mother52, rational quadratic, exponential ard, exponential squared ard, ardmatern32, ardmatern52 and rational quadratic ard) were optimized with the basis function (constant, linear and zero) for each output, then the one that gives the best performance is selected based on statistical evaluation criteria.

The development method of each GPR model has been designed in detail in Figure 13, including the interval which has been fixed for each parameter of the model and also for the agoriyhme of DA.

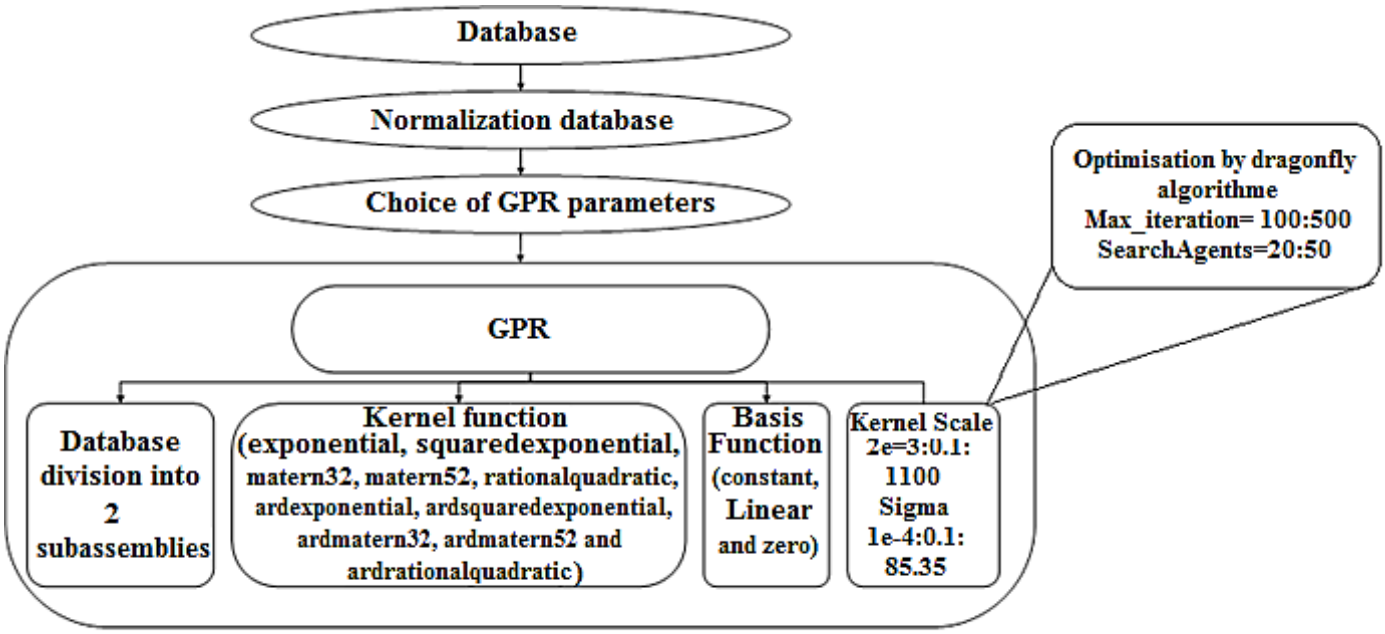

Figure 13– Organization chart for the development and optimization of the GPR architecture

The best models for the three outputs and their parameters (kernel scale and sigma) are presented in Table 7. It shows the coefficients (**R**, **R^2 and R^2_{adj}**) and performance measures (**RMSE, MSE, EPM, ESP and MAE)** for the learning and validation data sets, as well as the kernel parameters (Kernel Scale [sigmaM, sigmaF] and sigma. It also shows the best kernel functions with the resulting basis functions, as well as the number of dragonfly agents and the number of iterations that produced the best models. Also, it shows the number of parameters of each best model obtained.

Table 7 – Performances of the different GPR models tested.

DA	**Max_iteration=100 SearchAgents_no=30**											
	Kernel function	***Basis Function***	***Kernel Scale***	***Sigma***	**Number of parameters**	**$R/R^2/R^2_{adj}$**			**RMSE/MSE/EPM/ ESP /MAE**		
Outp			**Sigm**	**Sig**		**Tra**	**VA**	**AL**	**Train**	**VAL**	**ALL**

uts (%)			aM	maF			in	L	L			
DOC	Exponential	*Constant*	2.2540	16.2636	0.1350	28	1.0000 1.0000 1.0000	0.9993 0.9987 0.9981	0.9999 0.9999 0.9999	0.0214 0.0005 0.0078 0.0275 0.0067	0.2407 0.0579 0.1432 0.2906 0.1253	0.1291 0.0167 0.0460 0.1628 0.0402
UV 254	Squared-			10.8919	0.6		0.9997 0.9994 0.9993	0.9981 0.9963 0.9947	0.9995 0.9989 0.9988	0.2243 0.0503 0.1935 0.3363 0.1230	0.3958 0.1567 0.4498 0.5840 0.3104	0.2834 0.0803 0.2658 0.4229 0.1758
	Exponential	*Constant*	0.8708		558	28						
Turbidity	ARD-Exponentia	*Constant*	1.9796 5.9102 0.0223	16.8308	0.1432	28	1.0000 1.0000 1.0000	0.9999 0.9997 0.9996	1.0000 0.9999 0.9999	0.0421 0.0018 0.02550 .0542 0.0205	0.2140 0.0458 0.2276 0.2659 0.1648	0.1191 0.0142 0.0825 0.1517 0.0612

From Table 7 we can see that all the models have very high statistical coefficients (all are almost 1) and also very low statistical errors (close to zero) on the training and validation data and also on all data. This shows the efficiency of the developed models.

Figure 14 presents the plots of model predictions against the experimental values of the models shown in Table 7.

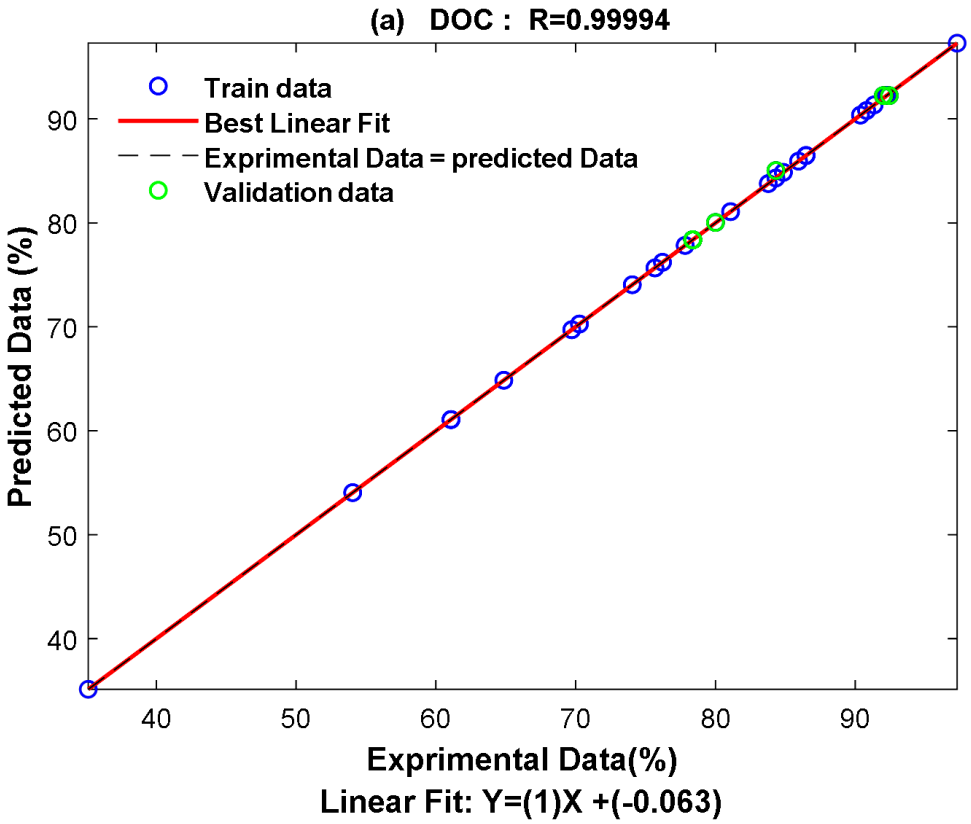

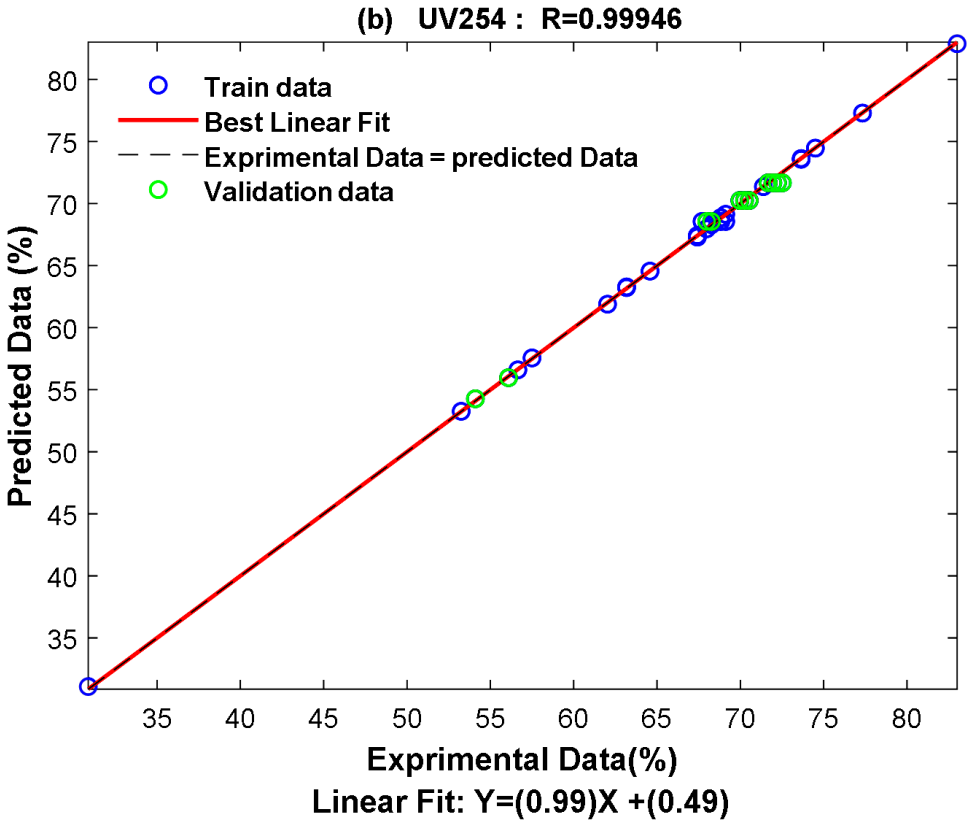

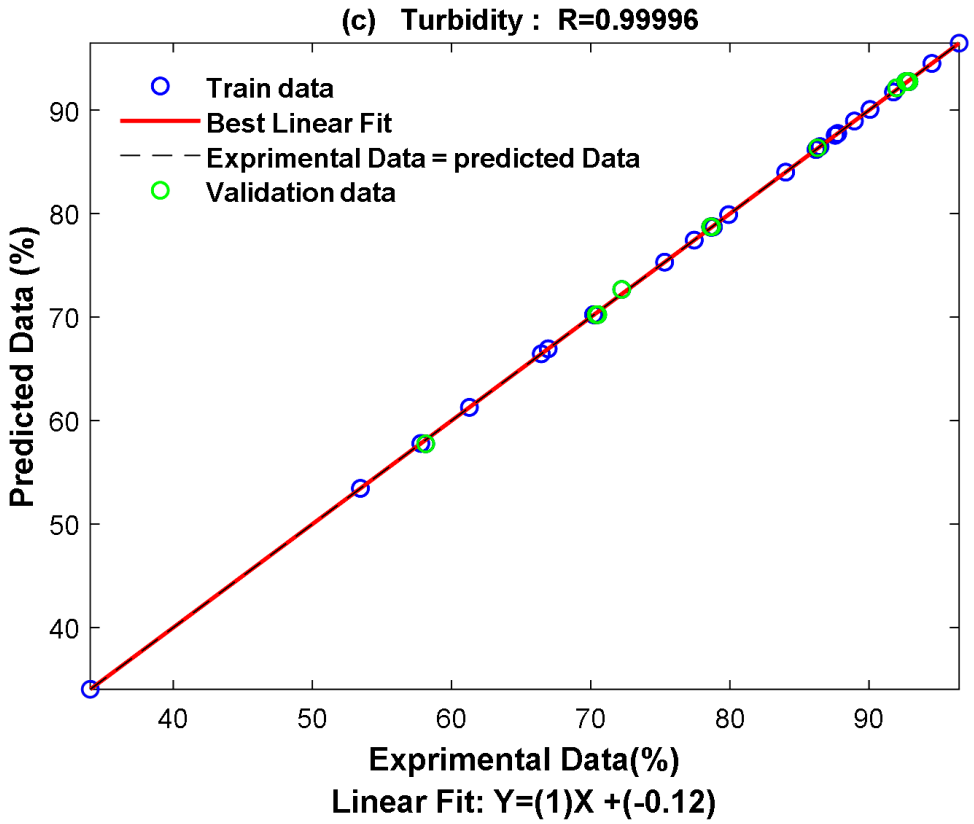

Figure 14 – Relationship between the experimental and the GPR-DA model predicted values: (a) DOC, (b) UV 254, and (c) Turbidity.

Figure 14 shows the excellent predictive capability of the developed GPR-DA models. Figure 15 plots the experimental data and model predictions at different samples. It can be seen that the model predictions are very close to the corresponding experimental values.

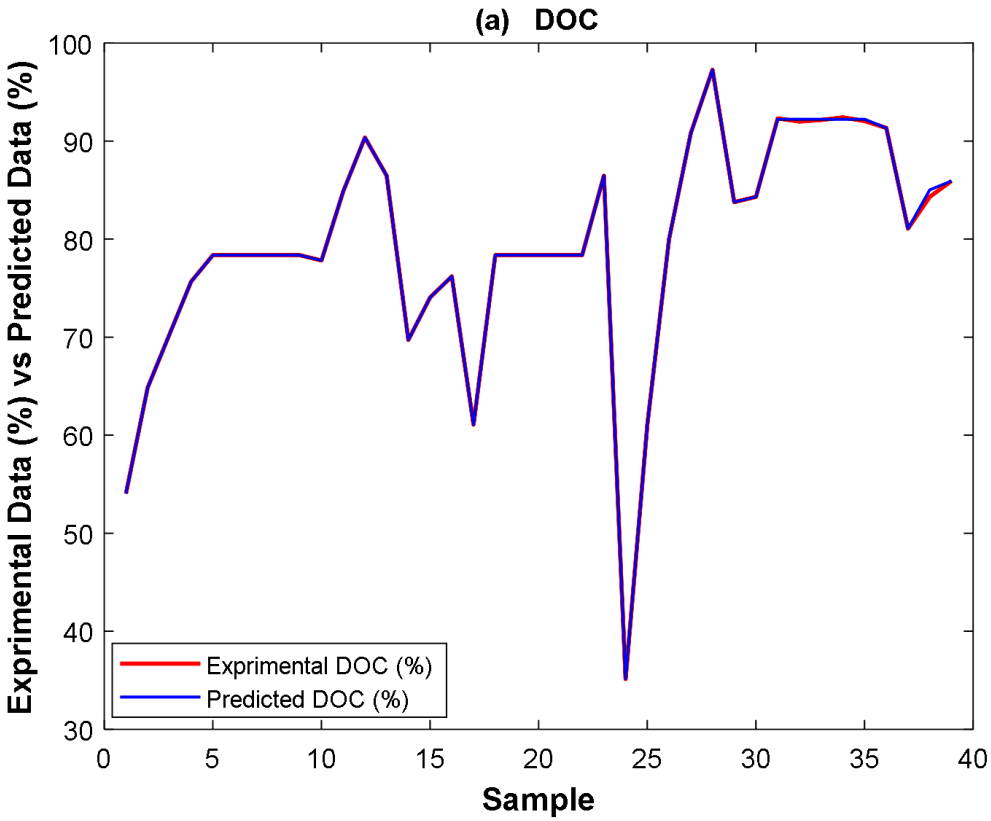

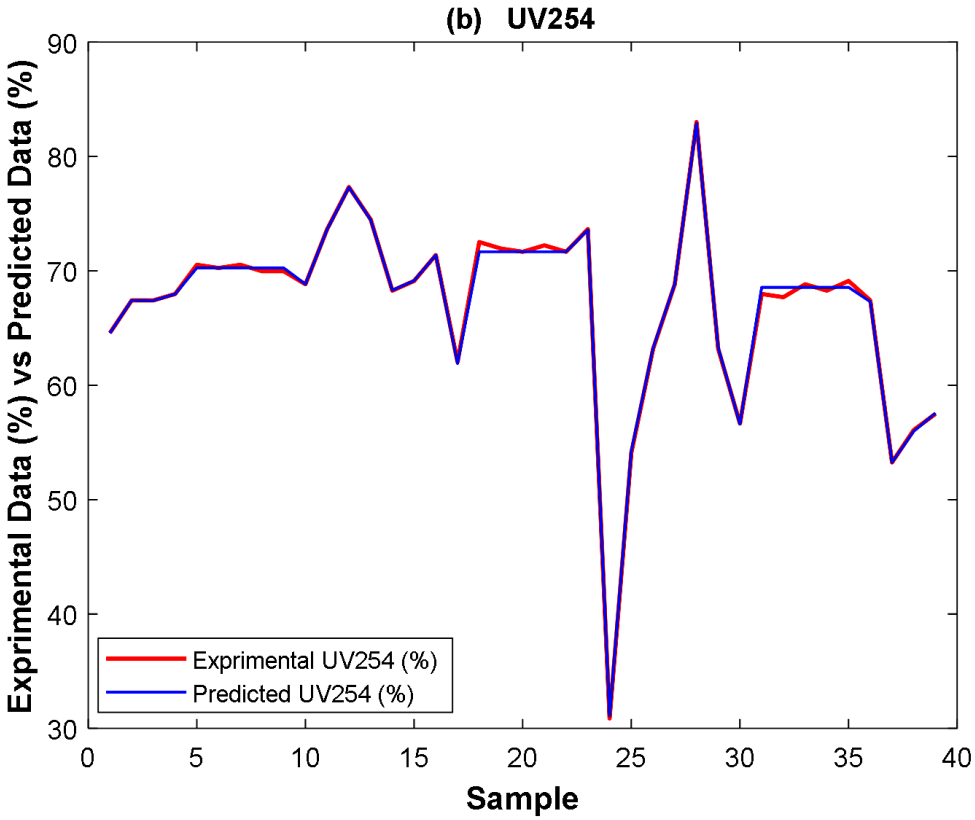

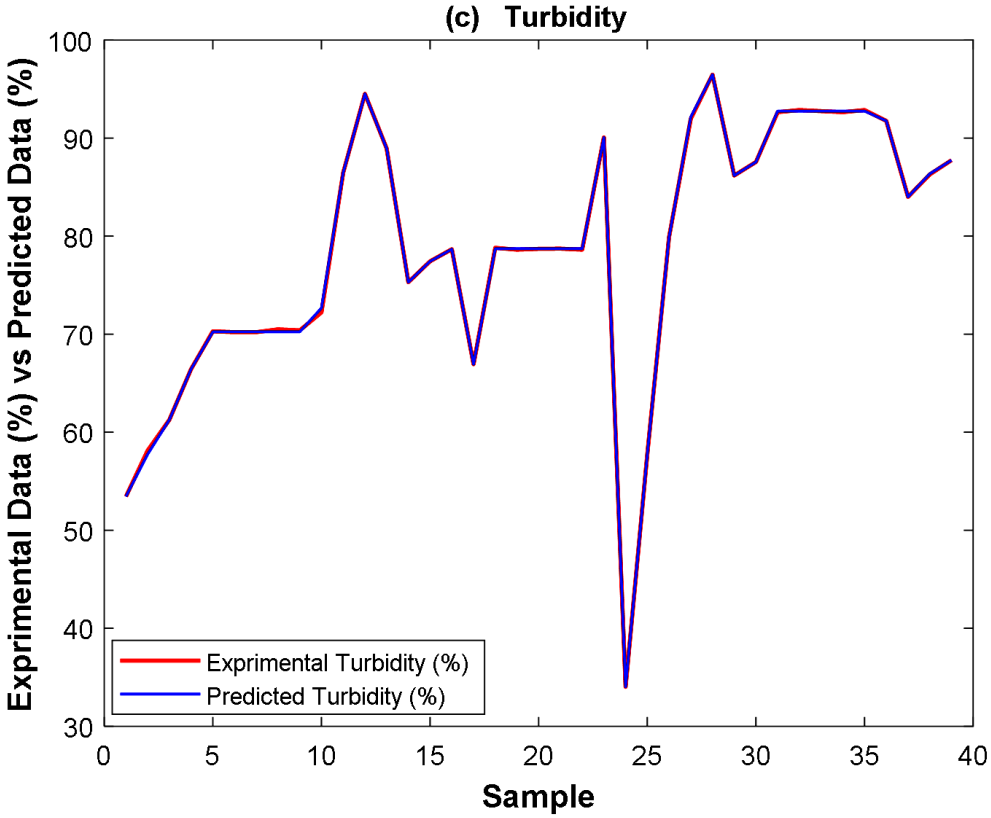

Figure 15 – experimental data and the predicted data of samples using GPR-DA model: (a) DOC, (b) UV 254, and (c) Turbidity.

3.3. Multi-objective optimization

The main objective of this optimization is to find the optimum wast water treatment condition, pH and dosage, in order to achieve the best treatment performance. For this, a MOO was used to solve this optimization problem. In this study, weightings are assigned to the 3 objectives and their weighted sum is used as a single objective which is then solved using the fmincon function available in the MATLAB Optimization Toolbox, the dragonfly algorithm (DA in MATLAB code), and the particle swarm algorithm (PSO in MATLAB code) available in the MATLAB Optimization Toolbox. For this, the maximum DOC removal rate (J_1), the maximum UV 254 removal rate (J_2) and the maximum turbidity removal rate (J_3) were considered as objective functions. They are then combined into a scalar goal as follows:

$$J = w_1 J_1 + w_2 J_2 + w_3 J_3$$

(23)

Where w_1, w_2 and w_3 are weighting factors, which can be calculated using the rank sum method (Dobrosz-Gómez et al., 2020; Einhorn and McCoach, 1977; Masouleh et al., 2022).

In this study, w_1, w_2 and w_3 are set to 0.34, 0.3 and 0.36 respectively. The resulting solution values of this optimization problem are given in Table 8.

Table 8 – Results of treatment efficiency (J) under optimal conditions based on DOC (J_1), UV254 (J_2) and turbidity (J_3).

	J_1 (%)	J_2 (%)	J_3 (%)	J (%)
$CuSO_4$				
• Fmincon_RSM, DA_RSM, PSO_RSM: $CuSO_4$ (dosage = 968.77 mg/L, pH = 11)				
• Fmincon_GPR, DA_GPR, PSO_GPR: $CuSO_4$ (dosage = 900 mg/L, pH = 11)				
RSM	90.54	76.60	92.03	86.90
GPR	90.36	77.29	94.51	87.94
$FeCl_3$				
• Fmincon_RSM, DA_RSM, PSO_RSM: $FeCl_3$ (dosage = 1000 mg/L, pH = 5.01)				
• Fmincon_GPR, DA_GPR, PSO_GPR: $FeCl_3$ (dosage = 1000 mg/L, pH = 5)				
RSM	87.38	76.00	90.85	85.22
GPR	86.47	73.57	90.06	83.92
$CuSO_4$ + $FeCl_3$				
• Fmincon_RSM, DA_RSM, PSO_RSM: $CuSO_4$ + $FeCl_3$ (dosage = 537.94 mg/L, pH = 5)				
• Fmincon_GPR, DA_GPR, PSO_GPR: $CuSO_4$ + $FeCl_3$ (dosage = 600 mg/L, pH = 5)				
RSM	96.47	80.54	96.00	91.52
GPR	97.28	82.88	96.47	92.71

The three MOO methods used (fmincon, DA and PSO) gave very similar optimization results for each treatment ($CuSo_4$, $Fecl_3$ and $CuSo_4$+$Fecl_3$) and each model (RSM and GPR). This shows the reliability of the models and the quality of the experimental results

obtained. Equally, this also shows the superiority of the mixed treatment compared to the two separate coagulants.

On the other hand, by comparing the optimization results from using the RSM model and the GPR model, it can be seen that they are very close. Identical results are obtained for the 2nd treatment (using $FeCl_3$). For the other two treatments, identical pH condition is obtained for optimization with both models, but there are some difference in the optimal dosage obtained. However, these slight difference between the optimal doses of coagulant did not influence the efficacy of the treatment with regard to the results obtained by the MOO methods (fmincon, DA and PSO) (Table 8). Returning to the interpretation of the results of the RSM, it can be seen that the coagulant dosage of the 1st treatment ($CuSo_4$) and of the 3rd treatment ($CuSo_4$+$Fecl_3$) have quadratic effects. Where, the intervals of the quadratic effects have approximately what was obtained by RSM and GPR, which confirms the proximity of the results. To confirm these results, an experimental validation method was applied.

3.4. Validation of the optimum conditions

In order to validate the optimization results, experiments were performed under the obtained optimal conditions to test the effectiveness of MOO based on RSM and GPR. These results have been presented in Table 9 in order to compare them to the predicted values and to express the error between them.

Where : $Error = Experimental\ response - Predicted\ response$ (24)

Table 9 – Comparison between actual and predicted response at optimum condition.

	Responses						
	J_1 (mg/L)	J_1 (%)	J_2	J_2 (%)	J_3 (NTU)	J_3 (%)	J (%)

RSM: $CuSO_4$ (dosage = 968.77 mg/L, pH = 11)							
GPR: $CuSO_4$ (dosage = 900 mg/L, pH = 11)							
Experimental (RSM)	1.81±0.080	90.20±0.440	0.079±0.003	77.71±0.668	2.87±0.032	93.61±0.072	87.60±0.39
Predicted response	1.74	90.54	0.082	76.60	3.57	92.03	86.90
Error_Exp_R	0.07±0.0	0.34±0.4	0.003±0.	1.110±0.	0.7±0.03	1.85±0.0	0.70±0.3
Experimental (GPR)	1.78±0.1	90.38±0.	0.080±0.	77.71±0.	2.46±0.0	94.52±0.	88.06±0.
Predicted response	1.78	90.36	0.080	77.29	2.46	94.51	87.94
Error_Exp_	0.00±0.1	0.02±0.59	0.00±0.00	0.42±0.32	0.00±0.0	0.01±0.10	0.12±0.16
RSM: $FeCl_3$ (dosage = 1000 mg/L, pH = 5.01)							
GPR: $FeCl_3$ (dosage = 1000 mg/L, pH = 5)							
Experimental (RSM/GPR)	2.50±0.1	86.49±0.	0.093±0.	73.56±0.	4.46±0.0	90.07±0.	83.92±0.409
Predicted response	2.33	87.38	0.084	76.00	4.10	90.85	85.22
Error_Exp_R	0.12±0.1	0.39±0.9	0.009±0.	2.44±0.4	0.36±0.0	0.78±0.0	1.32±409
Predicted response	2.50	86.47	0.093	73.57	4.46	90.06	83.92
Error_Exp_	0.00±0.1	0.02±0.92	0.00±0.00	0.01±0.99	0.00±0.0	0.01±0.09	0.00±0.40
RSM : $CuSO_4$ + $FeCl_3$ (dosage = 537.94 mg/L, pH = 5)							
GPR: $CuSO_4$ + $FeCl_3$ (dosage = 600 mg/L, pH = 5)							
Experimental (RSM)	0.55±0.03	97.01±0.14	0.062 ±0.003	82.43±0.925	1.69±0.045	96.24±0.001	92.35±0.355
Predicted response	0.65	96.47	0.068	80.54	1.79	96.00	91.52
Error_Exp_R	0.1±0.03	0.54±0.1	0.006±0.	1.89±0.9	0.1±0.04	0.24±0.0	0.83±0.3
Experimental (GPR)	0.50±0.0	97.32±0.	0.060±0.	82.90±0.	1.58±0.0	96.47±0.	92.68±0.
Predicted response	0.50	97.28	0.060	82.88	1.58	96.47	92.71
Error_Exp_	0.00±0.0	0.04±0.14	0.00±0.00	0.02±0.43	0.00±0.0	0.00±0.00	0.03±0.39

From Table 9, it was found that in each case the error was less than 3%. The DOC removal rate error in the three treatments is not higher than 0.54% for the two models (RSM and GPR). The maximum error of DOC elimination rate in the three treatments is 2.44% for

the two models (RSM and GPR). The error of turbidity elimination rate in the two models (RSM and GPR) based on the three treatments is not higher than 1.85%. Finally, the maximum error of the processing efficiency according to the two models used (RSM and GPR) is 1.32%.

From these experimental validation results, it can be seen that the results obtained by the two models are almost equal. This clearly reveals that the two models (RSM and GPR) developed for coagulation and flocculation are in good agreement with the experimental results, with a slight superiority of GPR model to the quadratic RSM model.

As the results are almost identical but with less errors for the GPR model, it is preferable to use the optimal conditions obtained by the GPR model. On the other hand, if one wants to reduce the operating costs, it is preferable to use the RSM model as a model which carries only five parameters at most compared to the GPR model which carries 28 parameters.

3.5. Interface for optimization and predictiont

To provide a simple way to implement MOO and to predict DOC, UV254, turbidity and treatment efficiency, an interface was designed using the MATLAB guide for the purpose of optimization and prediction (Figure 16). This interface to a tool has been converted into an exuctable application on windwos. This powerful application for direct use to predict outputs by selecting desirable pH values, coagulant dosage and even type of coagulation by RSM and also by GPR. On the other hand, the application will also make it possible to find a MOO solution to find the optimum pH and dosage for each type of coagulant according to the two models (RSM and GPR) by three methods (fmincon, DA and PSO).

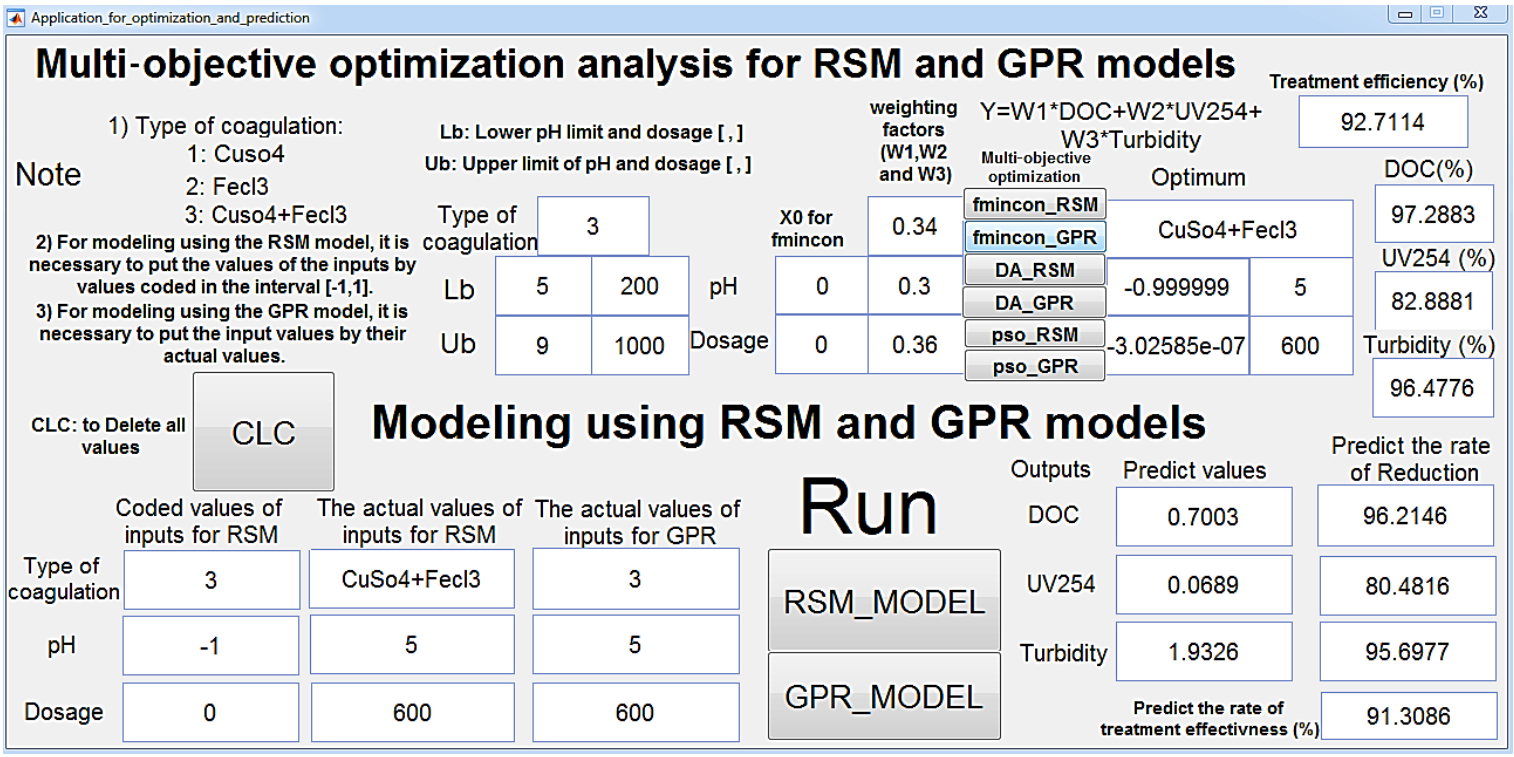

Figure 16 – Application à base une Interface de MATLAB for MOO (fmincon, DA and PSO), and predictiont DOC, UV 254, Turbidity and Treatment efficiency using RSM and GPR .

4. Conclusions

Coagulation and flocculation have been used to remove toxins from wastewater from the Pharmaceutical Effluent Treatment Plant. Coagulants copper sulfate, ferric chloride and a combination of cupric sulfate and ferric chloride in a ratio of 1:1 (CuSO4 + FeCl3) are used for the treatment process. The composite design approach has been used to improve independent process parameters such as pH and coagulant dosage in conjunction with DOC reduction, UV 254 and turbidity as dependent variables. On the other hand, the Gaussian process regression coupled with dragonfly algorithm is also used to model the three outputs, after combining the RSM databases of each coagulant in a single database. The evaluation of the best developed model is carried out by the experimental validation of optimal conditions of each treatment. For this, the MOO technique is used to determine the optimal conditions.

The experimental validations of the optimal treatment condition show the superiority of the GPR_DA model compared to RSM. The error obtained by experimental validation of the GPR_DA model is much lower than that obtained by the quadratic model of RSM. In addition, the results obtained show that the combined coagulant (CuSO4 + FeCl3) outperforms a single coagulant, CuSO4 or FeCl3. The efficiency measures of pretreatment with CuSO4, FeCl3, and (CuSO4 + FeCl3) are 88.06% (at dosage of 900 mg/L and pH of 11), 83.92% (at dosage of 1000 mg/L /L and pH of 5), and 92.68% (at a dosagee of 600 mg/L and pH of 5), respectively.

From the results obtained, it can be concluded that:

- Pretreatment by coagulation and flocculation of pharmaceutical effluents is well suited to mixed coagulant (CuSO4 + FeCl3).
- The GPR-DA models show great efficiency and profermence in predicting COD, UV254 and turbidity reduction rates, especially they can predict the reduction rates of the dependent parameters for the three treatments at the same time.

References

Adesina, O.A., Abdulkareem, F., Yusuff, A.S., Lala, M., Okewale, A., 2019. Response surface methodology approach to optimization of process parameter for coagulation process of surface water using Moringa oleifera seed. South African Journal of Chemical Engineering 28, 46–51.

Ashraf, M.I., Ateeb, M., Khan, M.H., Ahmed, N., Mahmood, Q., Zahidullah, 2016. Integrated treatment of pharmaceutical effluents by chemical coagulation and ozonation. Separation and Purification Technology 158, 383–386. https://doi.org/10.1016/j.seppur.2015.12.048

Belsley, D.A., Kuh, E., Welsch, R.E., 1980. Regression diagnostics: identifying influential data and sources of collinearity. Wiley.

Benitez, F.J., Acero, J.L., Gonzalez, T., Garcia, J., 2001. Ozonation and biodegradation processes in batch reactors treating black table olives washing wastewaters. Industrial & engineering chemistry research 40, 3144–3151.

Boldrini, C.L., Manfredi, N., Perna, F.M., Trifiletti, V., Capriati, V., Abbotto, A., 2017. Dye-Sensitized Solar Cells that use an Aqueous Choline Chloride-Based Deep Eutectic Solvent as Effective Electrolyte Solution. Energy Technology 5, 345–353.

Bousselma, A., Abdessemed, D., Tahraoui, H., Amrane, A., 2021. Artificial Intelligence and Mathematical Modelling of the Drying Kinetics of Pre-treated Whole Apricots. Kemija u industriji 70, 651–667.

Carvalho, M.N., Da Motta, M., Benachour, M., Sales, D.C.S., Abreu, C.A.M., 2012. Evaluation of BTEX and phenol removal from aqueous solution by multi-solute adsorption onto smectite organoclay. Journal of hazardous materials 239, 95–101.

Changotra, R., Rajput, H., Dhir, A., 2019a. Treatment of real pharmaceutical wastewater using combined approach of Fenton applications and aerobic biological treatment. Journal of photochemistry and photobiology A: Chemistry 376, 175–184.

Changotra, R., Rajput, H., Paul Guin, J., Varshney, L., Dhir, A., 2019b. Hybrid coagulation, gamma irradiation and biological treatment of real pharmaceutical wastewater. Chemical Engineering Journal 370, 595–605. https://doi.org/10.1016/j.cej.2019.03.256

Chen, Z., Yang, B., Wen, Q., Chen, C., 2020. Evaluation of enhanced coagulation combined with densadeg-ultrafiltration process in treating secondary effluent: Organic micro-pollutants removal, genotoxicity reduction, and membrane fouling alleviation. Journal of Hazardous Materials 396, 122697. https://doi.org/10.1016/j.jhazmat.2020.122697

Cheng, D., Ngo, H.H., Guo, W., Chang, S.W., Nguyen, D.D., Liu, Y., Wei, Q., Wei, D., 2020. A critical review on antibiotics and hormones in swine wastewater: Water pollution problems and control approaches. Journal of hazardous materials 387, 121682.

Daud, N.M., Abdullah, S.R.S., Hasan, H.A., 2018. Response surface methodological analysis for the optimization of acid-catalyzed transesterification biodiesel wastewater pre-treatment using coagulation–flocculation process. Process Safety and Environmental Protection 113, 184–192.

Daud, Z., Awang, H., Nasir, N., Ridzuan, M.B., Ahmad, Z., 2015. Suspended solid, color, COD and oil and grease removal from biodiesel wastewater by coagulation and flocculation processes. Procedia-Social and Behavioral Sciences 195, 2407–2411.

Dobrosz-Gómez, I., Gómez García, M.Á., Gaviria, G.H., GilPavas, E., 2020. Mineralization of cyanide originating from gold leaching effluent using electro-oxidation: multi-objective optimization and kinetic study. J Appl Electrochem 50, 217–230. https://doi.org/10.1007/s10800-019-01392-1

Dolling, O.R., Varas, E.A., 2002. Artificial neural networks for streamflow prediction. Journal of Hydraulic Research 40, 547–554.

Einhorn, H.J., McCoach, W., 1977. A simple multiattribute utility procedure for evaluation. Behavioral Science 22, 270–282.

El-Din, M.G., Smith, D.W., 2002. Ozonation of kraft pulp mill effluents: process dynamics. Journal of Environmental Engineering and Science 1, 45–57.

Fatombi, J.K., Jossé, R.G., Wotto, V., Aminou, T., Coulomb, B., 2007. Paramètres physico-chimiques de l'eau d'Opkara traitée par les graines de Moringa oleifera. JOURNAL-SOCIETE OUEST AFRICAINE DE CHIMIE 23, 75.

Gadipelly, C., Pérez-González, A., Yadav, G.D., Ortiz, I., Ibáñez, R., Rathod, V.K., Marathe, K.V., 2014. Pharmaceutical industry wastewater: review of the technologies for water treatment and reuse. Industrial & Engineering Chemistry Research 53, 11571–11592.

Ganiyu, S.O., Van Hullebusch, E.D., Cretin, M., Esposito, G., Oturan, M.A., 2015. Coupling of membrane filtration and advanced oxidation processes for removal of pharmaceutical residues: a critical review. Separation and Purification Technology 156, 891–914.

Ghumra, D.P., Agarkoti, C., Gogate, P.R., 2021. Improvements in effluent treatment technologies in Common Effluent Treatment Plants (CETPs): Review and recent advances. Process Safety and Environmental Protection 147, 1018–1051. https://doi.org/10.1016/j.psep.2021.01.021

GROUPE, S., 2001. Biotechnologies à Saïdal.

HARRAT, N., 2013. Elimination de la matière organique naturelle dans une filière conventionnelle de potabilisation d'eaux de surface. Université Mohamed Khider–Biskra.

Ho, J.Y., Afan, H.A., El-Shafie, A.H., Koting, S.B., Mohd, N.S., Jaafar, W.Z.B., Sai, H.L., Malek, M.A., Ahmed, A.N., Mohtar, W.H.M.W., 2019. Towards a time and cost effective approach to water quality index class prediction. Journal of Hydrology 575, 148–165.

Hong, S.H., Lee, M.W., Lee, D.S., Park, J.M., 2007. Monitoring of sequencing batch reactor for nitrogen and phosphorus removal using neural networks. Biochemical Engineering Journal 35, 365–370.

Iguergaziz, N., Benamara, S., Boukhiar, A., Djallouli, F.-Z., Guebrili, A., Angar, N.-E., Bitam, A., 2019. Release characteristics of paracetamol and oleuropein from Mech-Degla date fruit tablets enriched and non-enriched with freeze-dried olive leaf extract. Chemical Engineering Communications 206, 524–534.

Jose, J., Philip, L., 2021. Continuous flow pulsed power plasma reactor for the treatment of aqueous solution containing volatile organic compounds and real pharmaceutical wastewater. Journal of Environmental Management 286, 112202. https://doi.org/10.1016/j.jenvman.2021.112202

Joss, A., Zabczynski, S., Göbel, A., Hoffmann, B., Löffler, D., McArdell, C.S., Ternes, T.A., Thomsen, A., Siegrist, H., 2006. Biological degradation of pharmaceuticals in municipal wastewater treatment: proposing a classification scheme. Water research 40, 1686–1696.

Kaya, Y., Bacaksiz, A.M., Bayrak, H., Gönder, Z.B., Vergili, I., Hasar, H., Yilmaz, G., 2017. Treatment of chemical synthesis-based pharmaceutical wastewater in an ozonation-anaerobic membrane bioreactor (AnMBR) system. Chemical Engineering Journal 322, 293–301.

Khouni, I., Louhichi, G., Ghrabi, A., Moulin, P., 2020. Efficiency of a coagulation/flocculation–membrane filtration hybrid process for the treatment of vegetable oil refinery wastewater for safe reuse and recovery. Process Safety and Environmental Protection 135, 323–341.

K'oreje, K.O., Vergeynst, L., Ombaka, D., De Wispelaere, P., Okoth, M., Van Langenhove, H., Demeestere, K., 2016. Occurrence patterns of pharmaceutical residues in wastewater, surface water and groundwater of Nairobi and Kisumu city, Kenya. Chemosphere 149, 238–244.

Kumar, A., Chang, B., Xagoraraki, I., 2010. Human health risk assessment of pharmaceuticals in water: issues and challenges ahead. International journal of environmental research and public health 7, 3929–3953.

Lalwani, J., Gupta, A., Thatikonda, S., Subrahmanyam, C., 2020. An industrial insight on treatment strategies of the pharmaceutical industry effluent with varying qualitative characteristics. Journal of Environmental Chemical Engineering 8, 104190. https://doi.org/10.1016/j.jece.2020.104190

Lapworth, D.J., Baran, N., Stuart, M.E., Ward, R.S., 2012. Emerging organic contaminants in groundwater: a review of sources, fate and occurrence. Environmental pollution 163, 287–303.

Lefnaoui, S., Moulai-Mostefa, N., 2014. Investigation and optimization of formulation factors of a hydrogel network based on kappa carrageenan–pregelatinized starch blend using an experimental design. Colloids and Surfaces A: Physicochemical and Engineering Aspects 458, 117–125.

López-Fernández, R., Martínez, L., Villaverde, S., 2012. Membrane bioreactor for the treatment of pharmaceutical wastewater containing corticosteroids. Desalination 300, 19–23.

Manssouri, I., El Hmaidi, A., Manssouri, T.E., El Moumni, B., 2014. Prediction levels of heavy metals (Zn, Cu and Mn) in current Holocene deposits of the eastern part of the Mediterranean Moroccan margin (Alboran Sea). IOSR Journal of Computer Engineering 16, 117–123.

Manssouri, I., Manssouri, M., El Kihel, B., 2011. FAULT DETECTION BY K-NN ALGORITHM AND MLP NEURAL NETWORKS IN A DISTILLATION COLUMN: COMPARATIVE STUDY. Journal of Information, Intelligence and Knowledge 3, 201.

Masouleh, S.Y., Mozaffarian, M., Dabir, B., Ramezani, S.F., 2022. COD and ammonia removal from landfill leachate by UV/PMS/Fe2+ process: ANN/RSM modeling and optimization. Process Safety and Environmental Protection 159, 716–726. https://doi.org/10.1016/j.psep.2022.01.031

Momeni, M.M., Kahforoushan, D., Abbasi, F., Ghanbarian, S., 2018. Using chitosan/CHPATC as coagulant to remove color and turbidity of industrial wastewater: optimization through RSM design. Journal of Environmental Management 211, 347–355.

Mu, L., Zhao, L., Liu, L., Yin, H., 2012. Elemental distribution and mineralogical composition of ash deposits in a large-scale wastewater incineration plant: a case study. Industrial & engineering chemistry research 51, 8684–8694.

Ng, K.K., Shi, X., Ong, S.L., Lin, C.-F., Ng, H.Y., 2016. An innovative of aerobic bio-entrapped salt marsh sediment membrane reactor for the treatment of high-saline pharmaceutical wastewater. Chemical Engineering Journal 295, 317–325.

Pal, P., 2018. Treatment and disposal of pharmaceutical wastewater: toward the sustainable strategy. Separation & Purification Reviews 47, 179–198.

Park, J., Lechevalier, D., Ak, R., Ferguson, M., Law, K.H., Lee, Y.-T., Rachuri, S., 2017. Gaussian process regression (GPR) representation in predictive model markup language (PMML). Smart and sustainable manufacturing systems 1, 121.

Prieto-Rodríguez, L., Oller, I., Klamerth, N., Agüera, A., Rodríguez, E.M., Malato, S., 2013. Application of solar AOPs and ozonation for elimination of micropollutants in municipal wastewater treatment plant effluents. Water research 47, 1521–1528.

Qian, F., He, M., Song, Y., Tysklind, M., Wu, J., 2015. A bibliometric analysis of global research progress on pharmaceutical wastewater treatment during 1994–2013. Environmental Earth Sciences 73, 4995–5005.

Qian, F., He, M., Wu, J., Yu, H., Duan, L., 2019. Insight into removal of dissolved organic matter in post pharmaceutical wastewater by coagulation-UV/H2O2. Journal of Environmental Sciences 76, 329–338. https://doi.org/10.1016/j.jes.2018.05.025

Rasmussen, C.E., Williams, C.K.I., 2006. Gaussian Processes for Machine Learning Cambridge. MA: the MIT Press.[Google Scholar].

Rawat, M., 2019. Performance evaluation of common effluent treatment plant (CETP) for heterogenous waste at Narela-Delhi (India). Performance evaluation.

Rifi, S.K., Souabi, S., El Fels, L., Driouich, A., Nassri, I., Haddaji, C., Hafidi, M., 2022. Optimization of coagulation process for treatment of olive oil mill wastewater using Moringa oleifera as a natural coagulant, CCD combined with RSM for treatment optimization. Process Safety and Environmental Protection 162, 406–418.

Rodier, J., Legube, B., Merlet, N., 2016. L'analyse de l'eau-10e éd. Dunod.

Rodrigueza, O., Peralta-Hernandeza, J.M., Goonetillekeb, A., Bandalac, E.R., 2016. Treatment technologies for emerging contaminants in water: A review.

Santhosh, C., Velmurugan, V., Jacob, G., Jeong, S.K., Grace, A.N., Bhatnagar, A., 2016. Role of nanomaterials in water treatment applications: a review. Chemical Engineering Journal 306, 1116–1137.

Santo, C.E., Vilar, V.J., Botelho, C.M., Bhatnagar, A., Kumar, E., Boaventura, R.A., 2012. Optimization of coagulation–flocculation and flotation parameters for the treatment of a petroleum refinery effluent from a Portuguese plant. Chemical Engineering Journal 183, 117–123.

Shahedi, A., Darban, A.K., Taghipour, F., Jamshidi-Zanjani, A., 2020. A review on industrial wastewater treatment via electrocoagulation processes. Current Opinion in Electrochemistry 22, 154–169. https://doi.org/10.1016/j.coelec.2020.05.009

Sher, F., Malik, A., Liu, H., 2013. Industrial polymer effluent treatment by chemical coagulation and flocculation. Journal of Environmental Chemical Engineering 1, 684–689. https://doi.org/10.1016/j.jece.2013.07.003

Singh, B., Kumar, P., 2020a. Pre-treatment of petroleum refinery wastewater by coagulation and flocculation using mixed coagulant: Optimization of process parameters using response surface methodology (RSM). Journal of Water Process Engineering 36, 101317. https://doi.org/10.1016/j.jwpe.2020.101317

Singh, B., Kumar, P., 2020b. Pre-treatment of petroleum refinery wastewater by coagulation and flocculation using mixed coagulant: optimization of process parameters using response surface methodology (RSM). Journal of Water Process Engineering 36, 101317.

Sreekanth, D., Sivaramakrishna, D., Himabindu, V., Anjaneyulu, Y., 2009. Thermophilic treatment of bulk drug pharmaceutical industrial wastewaters by using hybrid up flow anaerobic sludge blanket reactor. Bioresource Technology 100, 2534–2539.

Tahraoui, H., Amrane, A., Belhadj, A.-E., Zhang, J., 2022a. Modeling the organic matter of water using the decision tree coupled with bootstrap aggregated and least-squares boosting. Environmental Technology & Innovation 27, 102419.

Tahraoui, H., Belhadj, A.-E., Amrane, A., Houssein, E.H., 2022b. Predicting the concentration of sulfate using machine learning methods. Earth Science Informatics 1–22.

Tahraoui, H., Belhadj, A.E., Hamitouche, A.E., 2020. Prediction of the Bicarbonate Amount in Drinking Water in the Region of Médéa Using Artificial Neural Network Modelling. Kem. ind. (Online) 69, 595–602. https://doi.org/10.15255/KUI.2020.002

Tahraoui, H., Belhadj, A.-E., Hamitouche, A.-E., Bouhedda, M., Amrane, A., 2021a. Predicting the concentration of sulfate (So4 2–) in drinking water using artificial neural networks: A case study: Médéa-algeria. Desalination and Water Treatment 217, 181–194.

Tahraoui, H., Belhadj, A.-E., Moula, N., Bouranene, S., Amrane, A., 2021b. Optimisation and Prediction of the Coagulant Dose for the Elimination of Organic Micropollutants Based on Turbidity. Kemija u industriji 70, 675–691.

Tran, N.H., Urase, T., Ta, T.T., 2014. A preliminary study on the occurrence of pharmaceutically active compounds in hospital wastewater and surface water in Hanoi, Vietnam. CLEAN–Soil, Air, Water 42, 267–275.

Trinh, T.K., Kang, L.S., 2011. Response surface methodological approach to optimize the coagulation–flocculation process in drinking water treatment. Chemical Engineering Research and Design 89, 1126–1135. https://doi.org/10.1016/j.cherd.2010.12.004

Verma, S., Prasad, B., Mishra, I.M., 2010. Pretreatment of petrochemical wastewater by coagulation and flocculation and the sludge characteristics. Journal of Hazardous materials 178, 1055–1064.

Wu, J., Lan, Z., Lin, J., Huang, M., Huang, Y., Fan, L., Luo, G., Lin, Y., Xie, Y., Wei, Y., 2017. Counter electrodes in dye-sensitized solar cells. Chemical Society Reviews 46, 5975–6023.

Yarahmadi, H., Duy, S.V., Hachad, M., Dorner, S., Sauvé, S., Prévost, M., 2018. Seasonal variations of steroid hormones released by wastewater treatment plants to river water and sediments: Distribution between particulate and dissolved phases. Science of the Total Environment 635, 144–155.

Zhou, P., Su, C., Li, B., Qian, Y., 2006. Treatment of high-strength pharmaceutical wastewater and removal of antibiotics in anaerobic and aerobic biological treatment processes. Journal of Environmental Engineering 132, 129–136.

Declaration of interests

☒ The authors declare that they have no known competing financial interests or personal relationships that could have appeared to influence the work reported in this paper.

☐The authors declare the following financial interests/personal relationships which may be considered as potential competing interests: